CD38 expression by neonatal human naïve CD4$^+$ T cells shapes their distinct metabolic state and high regulatory T cell potential

Authors: Laura R. Dwyer[1,2], Sean Clancy[2], Victoire Gouirand[2], Charles Chien[3, 4], Elizabeth E. Rogers, MD[5,6], Scott P. Oltman, MS[5,7,8,9], Laura L. Jelliffe-Pawlowski, PhD, MS[5,7,8,9,10,11], Susan V. Lynch[12,13], Allon Wagner[3, 4, 14], Alexis J. Combes[15], Tiffany C. Scharschmidt[2]*

Affiliations:

[1] University of California, San Francisco, Biomedical Sciences Graduate Program, San Francisco, CA 94143, USA

[2] University of California, San Francisco, Department of Dermatology, San Francisco, CA 94143, USA

[3] Department of Electrical Engineering and Computer Sciences, University of California, Berkeley, CA 94720, USA

[4] Center for Computational Biology, University of California, Berkeley, CA 94720, USA

[5] Healthy Outcomes of Pregnancy for Everyone Research Consortium, University of California, San Francisco

[6] Department of Pediatrics, University of California, San Francisco

[7] Department of Epidemiology and Biostatistics, University of California, San Francisco

[8] Department of Global Health Sciences, University of California, San Francisco

[9] California Preterm Birth Initiative, University of California, San Francisco

[10] Rory Meyers College of Nursing, New York University, New York, NY

[11] EGG Healthy Pregnancy, San Francisco, California

[12] Division of Gastroenterology, University of California, San Francisco, USA

[13] Benioff Center for Microbiome Medicine, Department of Medicine, University of California, San Francisco, USA

[14] Department of Molecular and Cell Biology, University of California, Berkeley, CA 94720, USA

[15] University of California, San Francisco, Department of Pathology, San Francisco, CA 94143, USA

* Corresponding author: tiffany.scharschmidt@ucsf.edu

Abstract

Neonatal life is marked by rapid antigen exposure, necessitating establishment of peripheral immune tolerance via conversion of naïve $CD4^+$ T cells into regulatory T cells (Tregs). Here, we demonstrate that increased Treg differentiation by naive $CD4^+$ T cells from human cord blood versus adult blood is integrally linked to their unique metabolic profile and their elevated expression of the NADase, CD38. Early life naïve $CD4^+$ T cells demonstrate a metabolic preference for glycolysis, which directly facilitates their Treg generation. We reveal an age-dependent gradient in CD38 levels on naïve $CD4^+$ T cells and show that high CD38 expression contributes to both the glycolytic state and high Treg potential of neonatal $CD4^+$ T cells, effects that are mediated at least in part via the NAD-dependent deacetylase SIRT1. Thus, the early life window for peripheral tolerance in humans is critically enabled by the immunometabolic state of the naïve $CD4^+$ compartment.

Introduction

Neonatal life is marked by rapid exposure of naïve immune cells to an array of new antigens, both self-antigens in peripheral tissues as well as exogenous microbial and environmental antigens. Developing adaptive immune tolerance to these antigens is critical to avoid excessive inflammatory or allergic responses that would be detrimental to homeostasis in the developing tissues and overall growth[1,2]. The main cells responsible for establishment and maintenance of tolerance are regulatory T (Treg) cells, which express the transcription factor forkhead box protein 3 (FOXP3) in tandem with immune regulatory molecules, such as CTLA4 and CD25, and produce the key immunosuppressive cytokine IL-10[3,4]. Notably, fetal and neonatal naïve $CD4^+$ T cells have been shown to have a heightened capacity to differentiate into Tregs compared to their adult counterparts[5,6]. This neonatal preference for Treg differentiation and immune regulation, often referred to as the early life window of tolerance, has been demonstrated in both humans and mice[7–9]. Prior work has revealed higher expression of certain Treg-associated genes in human naïve $CD4^+$ T cells during fetal development[10], with a progressive decline of this signature in cord blood and adult blood naïve $CD4^+$ T cells[11], which may contribute to age-dependent differences in their function. However, many questions remain regarding the mechanisms supporting preferential early life generation of Tregs.

Metabolic pathways influence immune cell fate and function by directly modulating substrates needed for energy, protein and nucleotide production. They also impart key effects on cellular responses, for example through the role of nicotinamide adenine dinucleotide (NAD+) as a co-factor for the sirtuin family of histone deacetylases[12] or direct modifications of histones by lactate[13]. Thus far, most work has focused on examining the metabolic state of adult immune cells, with comparatively little attention paid to how this might differ in early life. Even so, some key overarching principles have emerged that can help inform hypotheses about the metabolism of early life naïve $CD4^+$ T cells[14]. Naïve cells are relatively quiescent and their low ATP needs are fulfilled primarily by mitochondrial oxidative phosphorylation (OXPHOS). With activation, T cells meet their heightened energy needs by rapidly increasing both OXPHOS and glycolysis, but their ATP dependency shifts towards glycolysis as a more immediate energy source. Finally, the transition into a memory state is paired with reduced glycolysis and a shift back to OXPHOS for energy generation[15,16]. One of the few studies to explore early life metabolism focused on neonatal $CD8^+$ T cells, identifying that an early life preference for glycolysis likely contributes to their preferential effector differentiation while limiting their ability to become memory cells[17]. Analogous studies to examine the metabolic state of neonatal naïve $CD4^+$ T cells have yet to be

performed, but are particularly important given the multiple paths open to naïve $CD4^+$ T cells, i.e. differentiation into Tregs or various helper T cell types such as a Th1, Th2, or Th17, and the long-term impact these early cell fate decisions have on overall adaptive immune function and tolerance.

CD38, also known as cyclic ADP ribose hydrolase, is a glycoprotein expressed both intra- and extracellularly on many cell types, including immune cells[18]. CD38 has been used as a marker of early T cell activation[19] as well as a marker for $CD8^+$ T cell exhaustion or metabolic dysfunction in the setting of chronic viral infection[20] or cancer[21,22]. It was also recently reported as a potential marker of recent thymic emigrants (RTEs) in humans[23]. CD38 has various cellular functions, among the most prominent of which is regulating NAD+ levels by catalyzing the synthesis of ADP ribose and cyclic ADP ribose (cADPR) from NAD+, depleting NAD+ levels[18,24]. CD38 also augments cellular calcium through cADPR's role as an endogenous Ca2+ mobilizing nucleotide[25] and facilitates tyrosine kinase activity downstream of TCR signaling via direct interaction of its cytoplasmic tail with the Lck SH2 domain[26]. Thus far, a few reports have connected CD38 levels to the metabolic state of adult T cells. In murine $CD4^+$ T cells, deletion of CD38 increased OXPHOS capacity[21]. Similarly, in human adult naïve $CD4^+$ T cells, pharmacological inhibition of CD38 via the compound 78c increased OXPHOS and mitochondrial mass[18]. Separately, one study computationally predicted that CD38 is positively associated with a pro-tolerance phenotype in murine Th17 cells[27]. Thus, existing evidence links CD38 expression to reduced OXPHOS dependence with potential implications for $CD4^+$ T cell function. However, its contribution to the distinct metabolic state and differentiation capacity of neonatal T cells has not been examined. CD38's enzymatic reduction of NAD+ levels, i.e. its NADase activity, has the potential to impact the metabolic and functional states of immune cells through altered activity of NAD-dependent acetylases, which can modulate chromatin structure or protein degradation[28]. Indeed, sirtuin 1 (SIRT1) is a prominent member of this NAD-dependent deacetylase family, which has been shown to shape mitochondrial biogenesis, influence autoimmunity, and even facilitate FOXP3 protein degradation[12,29–32]. This link offers a potential mechanism of how CD38 could impact the functional and metabolic state of early-life immune cells that merits further study.

Here, we aimed to build on and interconnect knowledge in these areas to define how the metabolic state of early life human naïve $CD4^+$ T cells shapes their capacity to support age-specific immune functions. We find that the unique metabolic state of neonatal naïve $CD4^+$ T

cells, i.e. their glycolytic preference, is intricately tied to high CD38 expression, and that both these age-specific features support their enhanced capacity for Treg differentiation. We further identify CD38's NADase function and downstream effects on SIRT1 activity as a central pathway mediating CD38's impact on neonatal $CD4^+$ T cell biology. Collectively, this data offers novel insight into a key time for immune education and function, and a new mechanism by which the early life window of tolerance may be reinforced in humans.

Results

Neonatal naïve $CD4^+$ T cells generate more Tregs upon stimulation than their adult counterparts

We first sought to assess the distinct functional capacity of naïve $CD4^+$ T cells from cord blood (CB) and adult blood (AB). To probe their differentiation potential in an unbiased manner, we provided T cell receptor (TCR) stimulation without added cytokines. Specifically, naïve $CD4^+$ T cells were isolated from thawed aliquots of CB and AB mononuclear cells via negative selection kit (EasySep™) then cultured in the presence of human anti-CD3 and anti-CD28 soluble antibodies (ImmunoCult™) for 96 hours with no added cytokines to the culture. Separate replicate wells were analyzed at interval time points by flow cytometry, revealing an increase of the activation marker, CD69, by 24 hours that was slightly higher for AB versus CB cells **(Figure S1A-B)**. Expression of Ki67, a marker of active cell cycling and proliferation, was initially equivalent between CB and AB with a relative increase seen in CB at later time points (**Figure S1A, S1C)**, consistent with prior literature suggesting the higher proliferative potential and TCR reactivity of early life T cells[33] . Our own staining for Nur77, a marker upregulated by TCR signaling, also revealed a slightly higher baseline mean fluorescence intensity (MFI) in CB (**Figure S1D**)**.** CB and AB naïve $CD4^+$ T cells also showed equivalent extracellular TCRβ expression (**Figure S1E**), suggesting roughly equivalent density of cell surface TCR. Most strikingly, however, examination of Treg-related markers revealed a progressive increase in the percentage of $FOXP3^+CD25^+$ cells in CB versus AB, which was statistically significant at 96 hours (**Figure 1A-B**). This same increase in CB $FOXP3^+CD25^+$ cells was also observed upon activation of CB versus AB naïve $CD4^+$ T cells by several other methods, including bead activation and plate coating with anti-CD3/CD28 antibodies (**Figure 1C**).

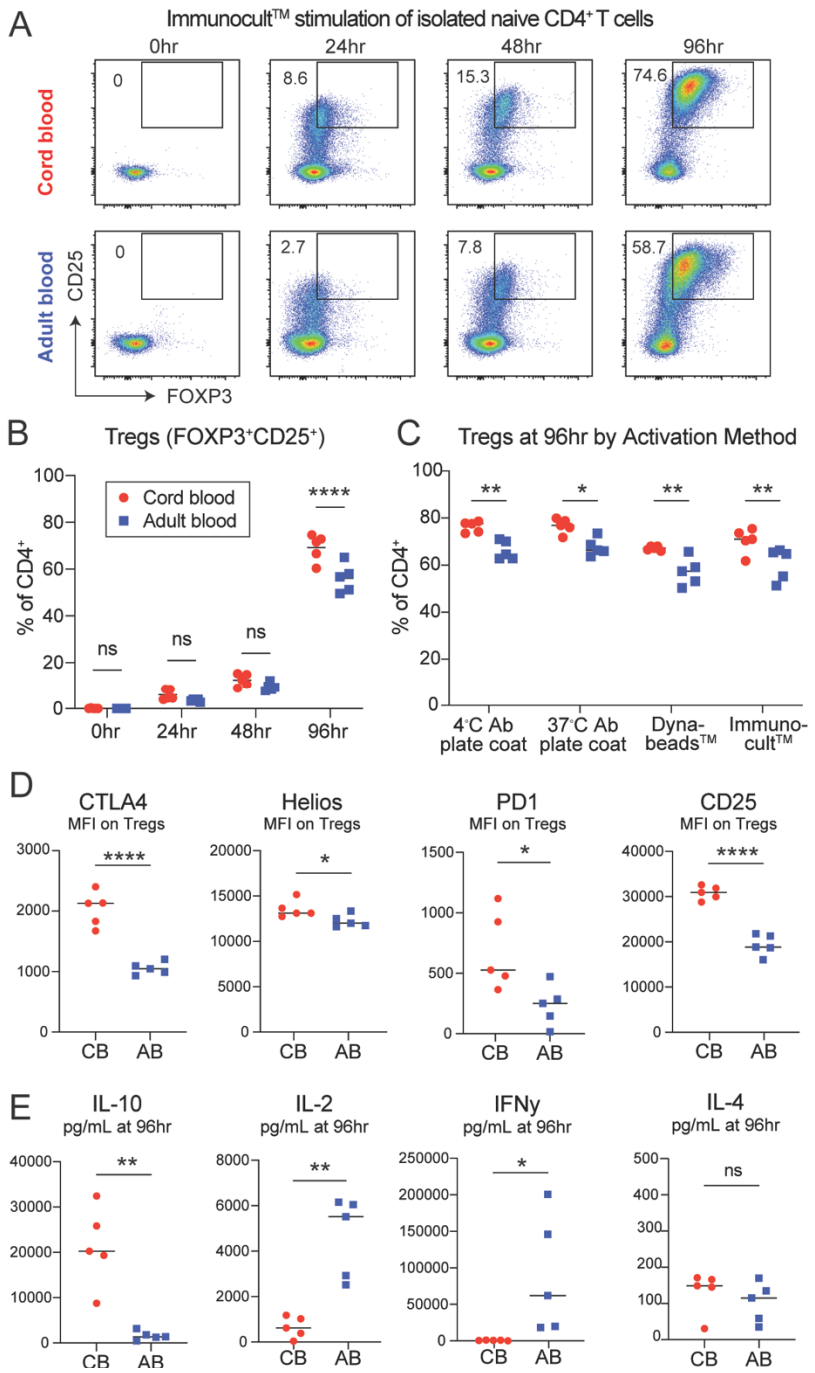

Figure 1: TCR stimulation of neonatal versus adult naïve CD4$^+$ T cells yields higher proportions of FOXP3$^+$CD25$^+$ Tregs (A, B) Representative flow plots and graph of the percentage of FOXP3$^+$CD25$^+$ (Tregs) from cord blood (CB) and adult blood (AB) naïve CD4$^+$ T cells at 0hr (non-stimulated) or 24, 48, and 96hr following stimulation with Immunocult™ anti-CD3/CD28 soluble antibodies with no added cytokines in culture. (C) Percentage of FOXP3$^+$CD25$^+$ (Tregs) from CB and AB naïve CD4$^+$ T cells at 96hr after TCR stimulation by different methods, including culture in a plate coated with anti-CD3/CD28 antibodies overnight at 4ºC, in a plate coated with anti-CD3/CD28 antibodies for 4hr at 37ºC, with beads added to culture coated in anti-CD3/CD28 (Dynabeads™), or with Immunocult™ anti-CD3/CD28 soluble antibodies. (D) Expression of various markers on FOXP3$^+$CD25$^+$ (Tregs) at 96hr after CB or AB naïve CD4$^+$ T cell stimulation, as measured by mean fluorescence intensity (MFI) by flow cytometry. (E) ELISA-based measurement of cytokines in cell culture supernatant of stimulated CB and AB naïve CD4$^+$ T cells at 96hr. All data points represent individual samples from different biological donors. For A, B, and D, one representative experiment of three is shown. For C and E one experiment was done and is shown.

FOXP3$^+$CD25$^+$ cells generated after CB versus AB naïve CD4$^+$ stimulation showed higher relative expression of several Treg effector molecules, including CTLA4, Helios, PD1 and CD25 (**Figure 1D, S1F**). While the percentage of FOXP3$^+$CD25$^+$ cells was increased at 96 hours in CB, the mean fluorescent intensity of FOXP3 was equivalent in this populations irrespective of age (**Figure S1G)**. FOXP3 and some other Treg-associated markers can be increased transiently on activated human CD4$^+$ T cells[34]. We thus performed ELISA on culture supernatants to profile functional cytokines secreted, which revealed increased levels of IL-10 in CB supernatant at 48 and 96 hours (**Figure 1E, S1I**). By comparison, AB culture supernatant contained more IL-2 and IFNγ, cytokines produced by activated CD4$^+$ effector T cells (**Figure 1E, S1I**). No significant differences were seen for IL-4 or IL-13 at either time point (**Figure 1E, S1H-I**). This indicated that FOXP3$^+$CD25$^+$ cells generated upon stimulation of CB naïve CD4$^+$ T cells represent induced Tregs with distinct properties from their adult counterparts. Collectively, this data demonstrates that upon stimulation, naïve CD4$^+$ T cells from CB versus AB have an increased capacity to become Tregs, even in the absence of specific Treg-stimulating cytokines.

Neonatal versus adult naïve CD4$^+$ T cells demonstrate a distinct transcriptional trajectory following stimulation

To uncover key drivers of this distinct functional response to stimulation, we designed a longitudinal experiment where RNA sequencing (RNA-seq) data was obtained from CB versus AB naïve CD4$^+$ T cells at baseline and three time points following activation (**Figure S2A**). To ensure purity of the input populations, naïve CD4$^+$ T cells (CD4$^+$ CD8^{neg} CD45RA$^+$ CD27$^+$ CCR7$^+$ CD95^{neg}) were isolated by FACS from CB and AB samples (**Figure S2B**). Cells were then either immediately harvested (0 hour) or first stimulated in culture with anti-CD3 and anti-CD28 soluble antibodies for 3, 24, or 48 hours. RNA-seq was then performed on these bulk cell populations, generating a dataset that could be mined for both baseline transcriptional differences and distinct age-dependent trajectories post activation.

Principal component analysis (PCA) was performed to visualize transcriptional differences between samples by time point and age (**Figure 2A**). PC1 encompassed 47.9% of variance and stratified samples longitudinally by time point, based on genes involved in cell proliferation and activation, e.g. CDC25A, MCM10, MKI67, IL2 (**Figure S2C**). PC2 13.2% variance separated CB from AB naïve CD4$^+$ T cells, with several of the axis-driving gene expression features having been previously reported to be differentially expressed by age or associated with development, e.g. SOX4[35], BCL11A[36], TSHZ2[10] (**Figure S2D, S2E**). A heatmap generated on the most

variable features revealed gene clusters with distinct patterns of expression based on CB versus AB status or time point (**Figure 2B**). Some clusters encompassed genes that varied between CB and AB, largely independent of activation status (2, 6, 8) whereas others showed dynamic increases (4, 5) or decreases (3, 7) in expression levels post-stimulation (**Figure 2C**). For example, Cluster 4 contained several cytokine genes that were lowly expressed at baseline or 3 hours, but had increased in either AB (IFNG) or CB (IL4, IL10, IL13) by 24 to 48 hours. Differential expression analysis between CB versus AB at each time point certain Treg-related genes that were already elevated in resting CB naïve $CD4^+$ T cells e.g. IKZF2, as previously reported[11], as well as others that increased only after stimulation (IL2RA, IL10, GATA3, PPARG, PDCD1). Conversely, consistent with our ELISA data, certain $CD4^+$ T effector genes were preferentially increased in AB with stimulation (IL2, IFNG) (**Figure 2D**). Gene set enrichment analysis (GSEA)[37,38] of ranked genes in resting naïve $CD4^+$ T cells showed AB enrichment in host defense and cytokine responses, with more subtle enrichment of development-related pathways in resting CB (**Figure S2F**). After 48 hours of stimulation, this developmental signature in CB was accompanied by enrichment for processes such as regulation of cell activation, adhesion and proliferation. Stimulated AB was instead enriched at 48 hours for terms related to defense against symbionts or virus, positive regulation of pattern recognition receptor signaling, and IL-17 production. (**Figure S2G**). Taken together, this analysis revealed a distinct transcriptional signature for CB cells both at baseline and up to 48 hours following activation, with features corroborating past work[10] (IKZF2) and our own flow data (HELIOS, IL-10) suggestive of a pro-tolerogenic signature in CB.

The transcriptome of neonatal naïve $CD4^+$ T cells suggests a distinct metabolic profile

Based on existing literature linking the metabolic state of neonatal naïve $CD8^+$ T cells to their differentiation trajectory and functional capacity[17,39], we next wanted to investigate if there were baseline differences in the metabolic state of CB and AB naïve $CD4^+$ T cells. Focused examination of our bulk RNA-seq dataset for differentially expressed metabolic genes revealed higher expression of certain glycolysis-related genes in CB at baseline (**Figure S2H**), hinting that neonatal naïve $CD4^+$ T cells also display a distinct metabolic profile. To corroborate this finding, we turned to an independent dataset previously published by Bunis et al., in which sorted CB and AB naïve $CD4^+$ T cells were subjected to single-cell RNA sequencing (scRNA-seq)[11]. Differential gene expression analysis validated our observation of upregulation of glycolysis-related genes in CB, and revealed a parallel downregulation of mitochondrial genes critical to oxidative phosphorylation (**Figure 2E**). To further characterize the metabolic profile of

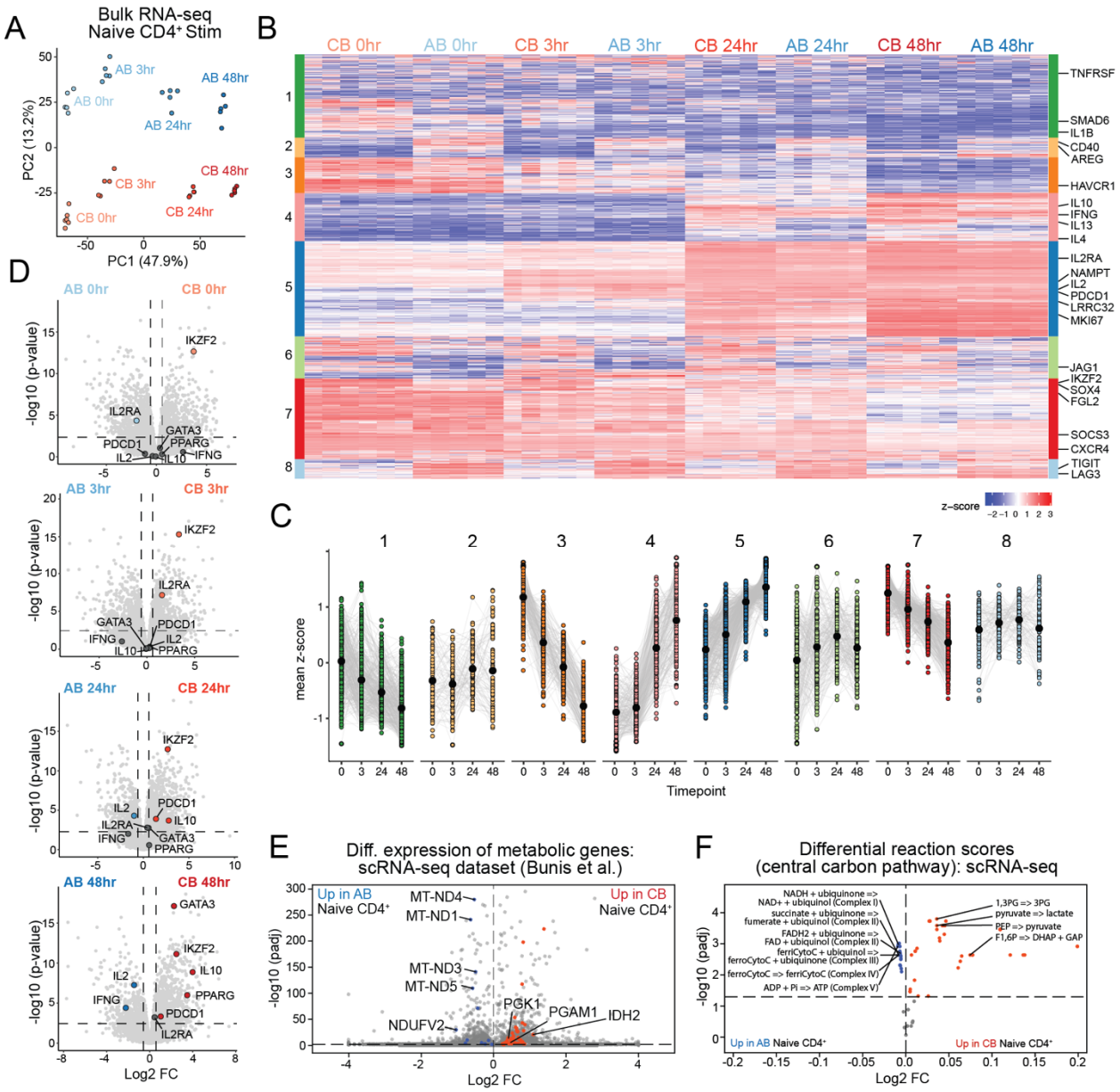

Figure 2: Transcriptomic data analysis and in-silico modeling of CB versus AB naïve CD4$^+$ T cells reveals unique functional and metabolic programs at baseline and after activation (A) PCA plot of bulk RNA-seq data from naïve CD4$^+$ T cells (CD4$^+$CD8^{neg}CD45RA$^+$CD27$^+$CCR7$^+$CD95^{neg}) sorted from CB and AB, with samples taken at baseline (0 hr), 3, 24 and 48 hr after stimulation. (B) Heatmap of top features (i.e. clusters of genes) with variable expression by age (CB versus AB), each cluster is denoted by a different color on x axis. (C) Mapping of cluster expression (mean z-score of each gene) over time. Black dots represent the mean z-score per time point. Colors correspond with labelled clusters in B. (D) Volcano plots of differential gene expression for CB versus AB naïve CD4$^+$ T cells at each time point, with specific genes related to Tregs or activated effector cells highlighted. Horizontal dotted line represents Benjamini-Hochberg adjusted p-value of 0.05. (E) Differential expression of key metabolic genes from re-analysis of published scRNA-seq dataset of CB versus AB naïve CD4$^+$ T cells (Bunis et al.). (F) Compass comparison of CB versus AB naïve CD4+ T cell metabolic states in central carbon metabolism reveals upregulation of core glycolysis reactions and an overall downregulation of the OXPHOS pathway in CB. Dots represent metabolic reactions, as annotated in the Human1 GEM metabolic model.

CB and AB blood naïve $CD4^+$ T cells, we turned to Compass, a flux-balance analysis algorithm that explicitly models the flow of metabolites through the metabolic network to characterize the metabolic state of cells[27]. Compass analysis of our own baseline bulk RNA-seq dataset did not reveal statistically significant pathways in CB versus AB. Thus, we leveraged the Bunis et al. scRNA-seq dataset, performing a Compass run on the central carbon pathways (glycolysis, TCA, and OXPHOS). To robustly capture the transcriptomic state of cells in face of inter-donor variation, we pseudobulked (averaged), the gene expression profiles of cells belonging to the same donor. Using these pseudobulk profiles, we discovered striking metabolic differences where glycolysis reactions were upregulated, while OXPHOS reactions across all complexes were downregulated in the CB group (**Figure 2F**). Thus, our metabolic-focused analyses of the transcriptional state of naïve $CD4^+$ T cells suggest that CB cells have a distinct baseline metabolic state, with a possible preference for glycolysis.

Neonatal naïve $CD4^+$ T cells are more reliant on glycolysis than their adult counterparts

To understand if these distinct neonatal versus adult naïve $CD4^+$ T cell transcriptional signatures reflected differences in metabolic function, we first used SCENITH[40], a flow cytometry-based approach that combines pharmacologic inhibition of metabolic pathways with a puromycin antibody-based readout of cellular ATP production (**Figure 3A**). SCENITH can measure both the pathway by which cells generate energy (i.e. glycolysis versus mitochondrial OXPHOS) as well as their preferred energy source (i.e. glucose versus fatty acid and amino acid oxidation). As metabolic state can be impacted by many exogenous factors, we first performed SCENITH on $CD4^+$ T cells prior to and after cryopreservation. This did not reveal significant differences in relative OXPHOS or glycolysis dependence between naïve $CD4^+$ T cells that were processed immediately after collection versus those initially frozen, then thawed and rested overnight prior to analysis (**Figure S3A**).

Based on these results, we opted to perform our metabolism-focused experiments on cryopreserved samples to enable parallel processing and analysis of multiple biological replicates from different CB and AB donors. First, we used SCENITH to compare naïve $CD4^+$ T cells from CB or AB at baseline, prior to activation. Mean puromycin fluorescence intensity was equivalent between groups in the absence of metabolic inhibition, suggesting relatively equivalent ATP use irrespective of age (**Figure S3B-C**). Changes to puromycin incorporation in the setting of various pathway inhibitors revealed CB naïve $CD4^+$ T cells to have an increased relative dependence on glycolysis versus AB, with a converse decrease in relative dependence

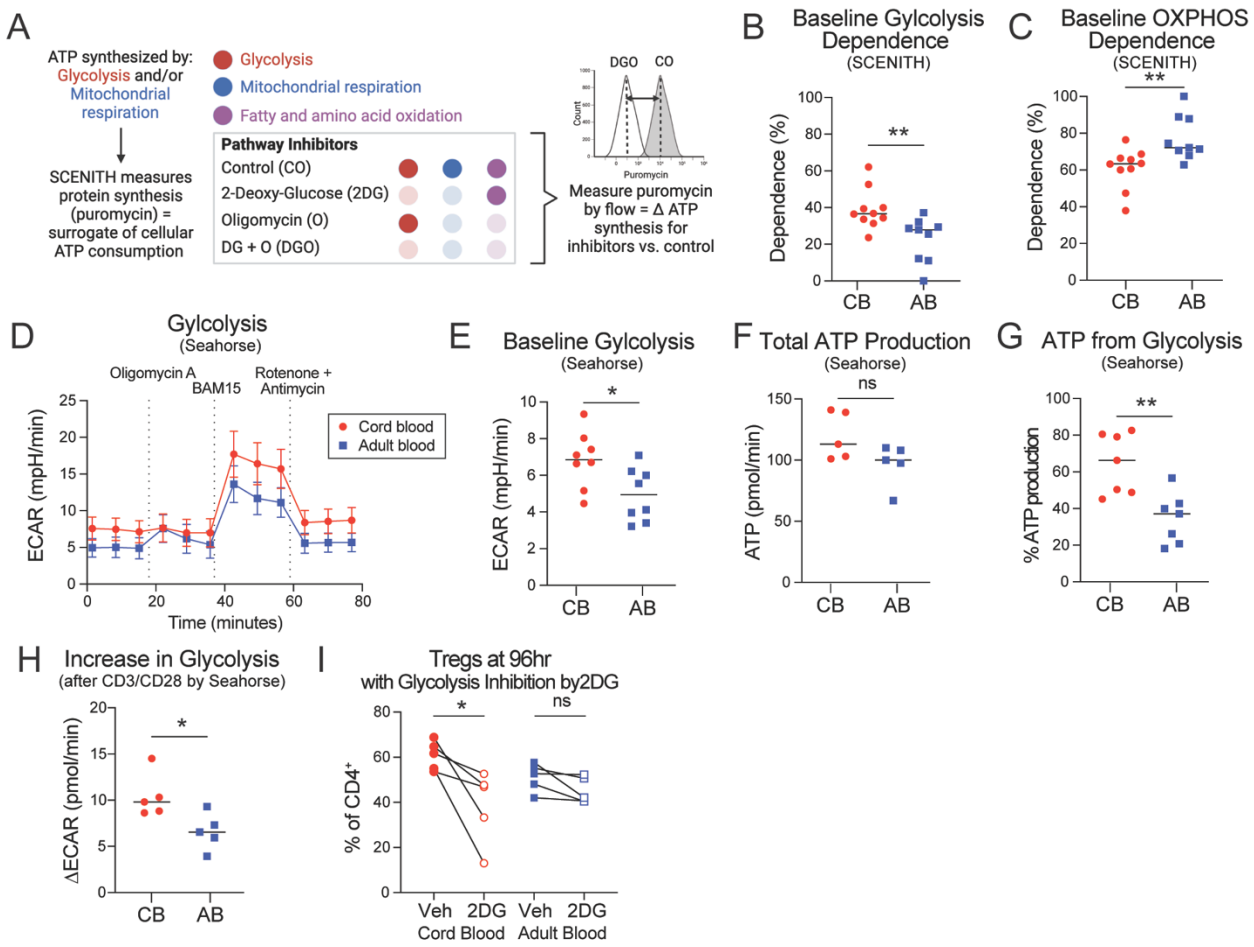

Figure 3: Neonatal naïve CD4$^+$ T cells demonstrate a metabolic preference for glycolysis (A) Schematic of SCENITH workflow (B,C) Baseline (non-activated) dependence on glycolysis and mitochondrial oxidative phosphorylation in cord blood (CB) and adult blood (AB) naive CD4$^+$ T cells measured via SCENITH. (D) Seahorse graph of ECAR (glycolysis) of baseline (non-activated) CB and AB naive CD4$^+$ T cells. (E) Quantification of baseline glycolysis between CB and AB naive CD4$^+$ T cells via Seahorse. (F) Total ATP production and (G) percent of ATP made from glycolysis for CB versus AB naive CD4$^+$ T cells via Seahorse. (H) The change in ECAR for CB and AB naive CD4$^+$ T cells after acute TCR activation via real-time introduction of anti-CD3/CD28 soluble antibodies in Seahorse plate reader, between via Seahorse. (I) Quantification of the percentage change in FOXP3$^+$CD25$^+$ (Tregs) from seen at 96 hours post Immunocult^{TM} stimulation of CB and AB naïve CD4$^+$ T cells with or without concurrent inhibition of glycolysis via treatment with 0.5mM 2DG for 24 hours prior to as well as during stimulation. Vehicle (Veh) control = DMSO. All data points represent individual samples from different biological donors. B, C, and E are two combined experimental replicates. D, H, and I are one representative experiment of two experimental repeats.

on OXPHOS (**Figure 3B-C**). We did not observe any differences in energy substrate preference by age, with both CB and AB naïve CD4$^+$ T cells demonstrating a higher reliance on fatty acid and amino acid oxidation versus glucose, as is expected for non-activated, resting cells (**Figure S3D-E**). We further took advantage of SCENITH's capacity to measure metabolism at single-cell resolution by examining the metabolic preferences of the FOXP3$^+$CD25$^+$ cells that were generated in CB and AB cultures at 96 hours post-activation. The Treg populations from CB and AB displayed no differences in metabolic dependencies, with both having a relatively higher

dependence on glycolysis compared to OXPHOS and a preference for glucose compared to fatty and amino acid oxidation (**Figure S3F-I).**

To validate our results from SCENITH and further measure the absolute level of energy pathway use between CB versus AB, we performed Seahorse on resting naïve $CD4^+$ T cells. This showed higher baseline extracellular acidification rate (ECAR) in CB cells, reflective of increased glycolysis (**Figure 3D-E**). Consistent with puromycin levels measured by SCENITH, Seahorse did not show an age-dependent difference in total ATP generation by naïve $CD4^+$ T cells, but a relative increase in ATP made from glycolysis in CB was confirmed (**Figure 3F-G**). Seahorse did not reveal differences in baseline oxygen consumption rate (OCR, measurement of OXPHOS), ATP from OXPHOS, or spare respiratory capacity between ages (**Figure S3J-M**). Taking advantage of the Seahorse Human T cell Activation Assay, we also were able to measure ECAR and OCR continuously in the two hours following anti-CD3/CD28 activation with Immunocult™. This showed that CB naïve $CD4^+$ T cells increase their glycolytic activity even more than AB following TCR stimulation, which was matched in this setting by age-specific increases in OXPHOS (**Figure 3H, S3N-P**).

Considering the integral relationship between cell metabolism and function, we next probed whether the glycolytic state of CB naïve $CD4^+$ T cells was linked to their observed heightened capacity for Treg generation. For this, we employed 2-deoxy-D-Glucose (2DG), a pharmacological inhibitor of glycolysis, which we first titrated to a dose that did not impact $CD4^+$ cell viability, proliferative capacity (Ki67) or activation (CD69) during 96 hour stimulation (**Figure S3Q-S**). We then treated CB and AB naïve $CD4^+$ T cells with 0.5mM of 2DG during concurrent stimulation with ImmunoCult™ anti-CD3/CD28 antibodies, before measuring Treg generation at 96 hours. 2DG treatment led to a reduction in the percentage of $FOXP3^+CD25^+$ cells generated from CB naïve $CD4^+$ T cells without analogous effects on AB (**Figure 3I**). Taken together, this data reveals a unique metabolic state for CB naïve $CD4^+$ T cells at baseline and connects an increase in glycolytic dependency with their ability to become Tregs.

CD38 is highly expressed on naïve $CD4^+$ T cells in early life

To uncover potential biological drivers of the distinct CB and AB metabolic and functional states, we returned to our RNA-seq analysis of these cell prior to TCR stimulation. Among the top differentially expressed genes metabolically related genes was CD38, which had roughly 4-fold higher expression in CB versus AB naïve $CD4^+$ T cells (**Figure 4A**). Extracellular staining for

CD38 by flow cytometry confirmed elevated protein-level expression broadly on lymphocyte populations from CB versus AB (**Figure 4B, S4A**). Notably though, CD38 expression was highest on CB naïve $CD4^+$ T cells followed by Tregs (**Figure 4C**). CD38 expression on naïve $CD4^+$ T cells was measured by both extracellular staining alone as well as extracellular and intracellular staining together to confirm the increase in CB expression was not due to internalization of CD38 in AB cells but instead overall expression. (**Figure S4B**). To validate whether elevated CD38 expression reflects a unique cord blood state or extends into the early life window, we obtained peripheral blood from prematurely born infants aged 6 weeks. CD38 staining showed intermediate levels on neonatal naïve $CD4^+$ T cells as compared to CB and AB cells, suggesting an age-dependent gradient of CD38 expression (**Figure 4D**). Examining patterns of CD38 staining after CB and AB naïve $CD4^+$ T cell anti-CD3/CD28 stimulation, we saw an initial increase at 3 hours, consistent with its use as a marker of recent cell activation[18], followed by a gradual decrease over the next 4 days of culture (**Figure S4C**). Interestingly, CD38 was even higher on de novo generated Tregs in both CB and AB as compared to non-Tregs at 24 and 48 hours after activation, with CB Tregs showing the highest expression (**Figures 4E, S4D**). Thus, CD38 levels are increased on early life naïve $CD4^+$ T cells as well as on Tregs generated by TCR stimulation.

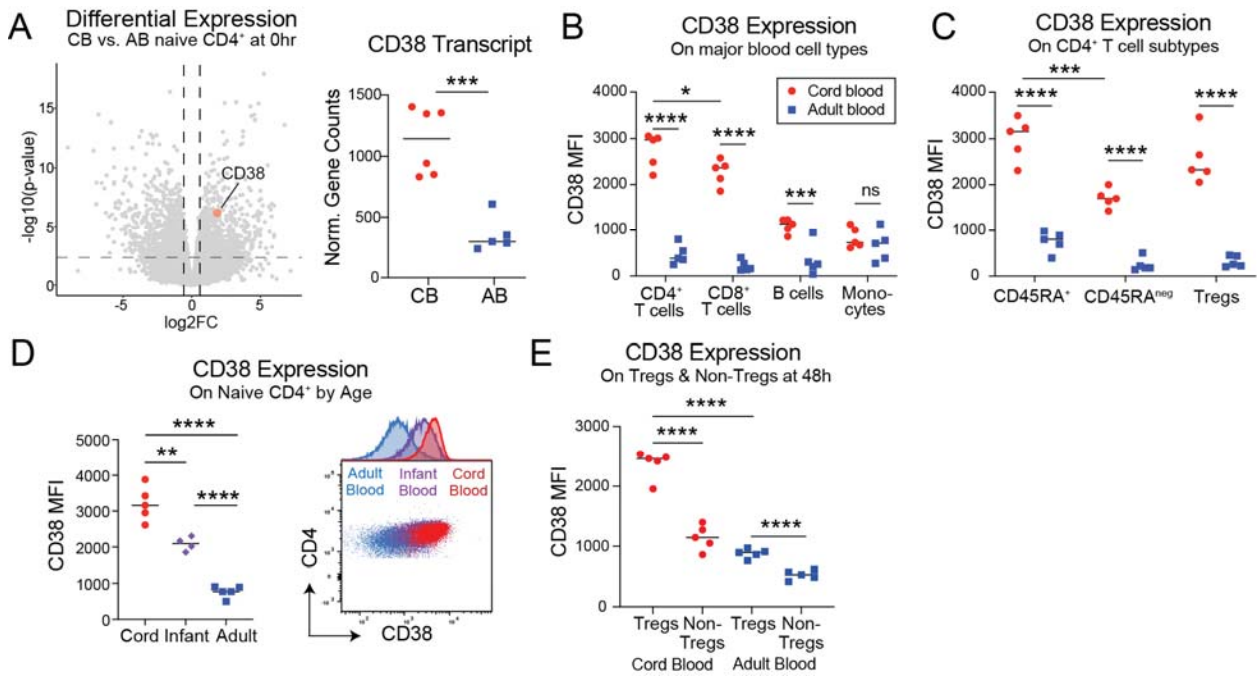

Figure 4: CD38 expression is highly enriched on naïve CD4$^+$ T cells in early life (A) Volcano plot highlighting CD38 from RNA-seq of CB versus AB naive CD4$^+$ T cells (non-activated = 0hr) and normalized gene counts of CD38. (B) Mean fluorescent intensity (MFI) of surface CD38 measured by flow cytometry on various immune cell populations (CD4$^+$ T cells, CD8$^+$ T cells, B cells, and monocytes) in non-activated peripheral adult and cord blood. (C) CD38 MFI on CD4$^+$ T cell subsets (CD45RA$^+$, CD45RA^{neg} and FOXP3$^+$CD25$^+$ Tregs) in non-activated peripheral cord blood (CB) and adult blood (AB). (D) CD38 MFI on naïve CD4$^+$ T cells from CB, peripheral blood from 6 week-old preterm infants, or AB. (E) CD38 MFI on CD4$^+$ FOXP3$^+$CD25$^+$ (Tregs) and FOXP3^{neg}CD25^{neg} (non-Tregs) seen in culture at 48 hours after Immunocult^{TM} activation of naïve CD4$^+$ T cells from CB or AB. All data points represent individual samples from different biological donors. B, C, and E show one representative experiment from two experimental replicates. D shows one experiment.

CD38 inhibition impedes glycolysis and Treg generation by CB naïve CD4$^+$ T cells

To dissect if CD38 expression on CB versus AB naïve CD4$^+$ T cells was functionally linked with their heightened Treg potential, we took advantage of the potent and specific CD38 pharmacological inhibitor, 78c[18,41], incubating CB and AB naïve CD4$^+$ T cells with 10uM 78c for 24 hours prior to activation as well as in the 4 days following TCR stimulation. This level of CD38 inhibition resulted in significantly decreased Treg generation by CB naïve CD4$^+$ T cells without analogous effects on AB Tregs (**Figures 5A-B**) or any impact on CD4$^+$ T cell proliferation (Ki67) or activation (CD69) (**Figures 5C-D, S5A**). Titration of 78c in our culture conditions revealed already maximal CB Treg inhibition at 5uM, whereas significant decreases in AB Treg generation were not seen until 20-40uM, doses at which we also saw decreased Ki67 (**Figure S5B-C**). Treatment of CB with 5uM 78c also led to a reduction in CTLA4 expression on Tregs generated from CB but not AB (**Figure 5E, S5D**), and decreased IL-10 in CB cell supernatant at 96h without accompanying changes in IL-2 (**Figure 5F**).

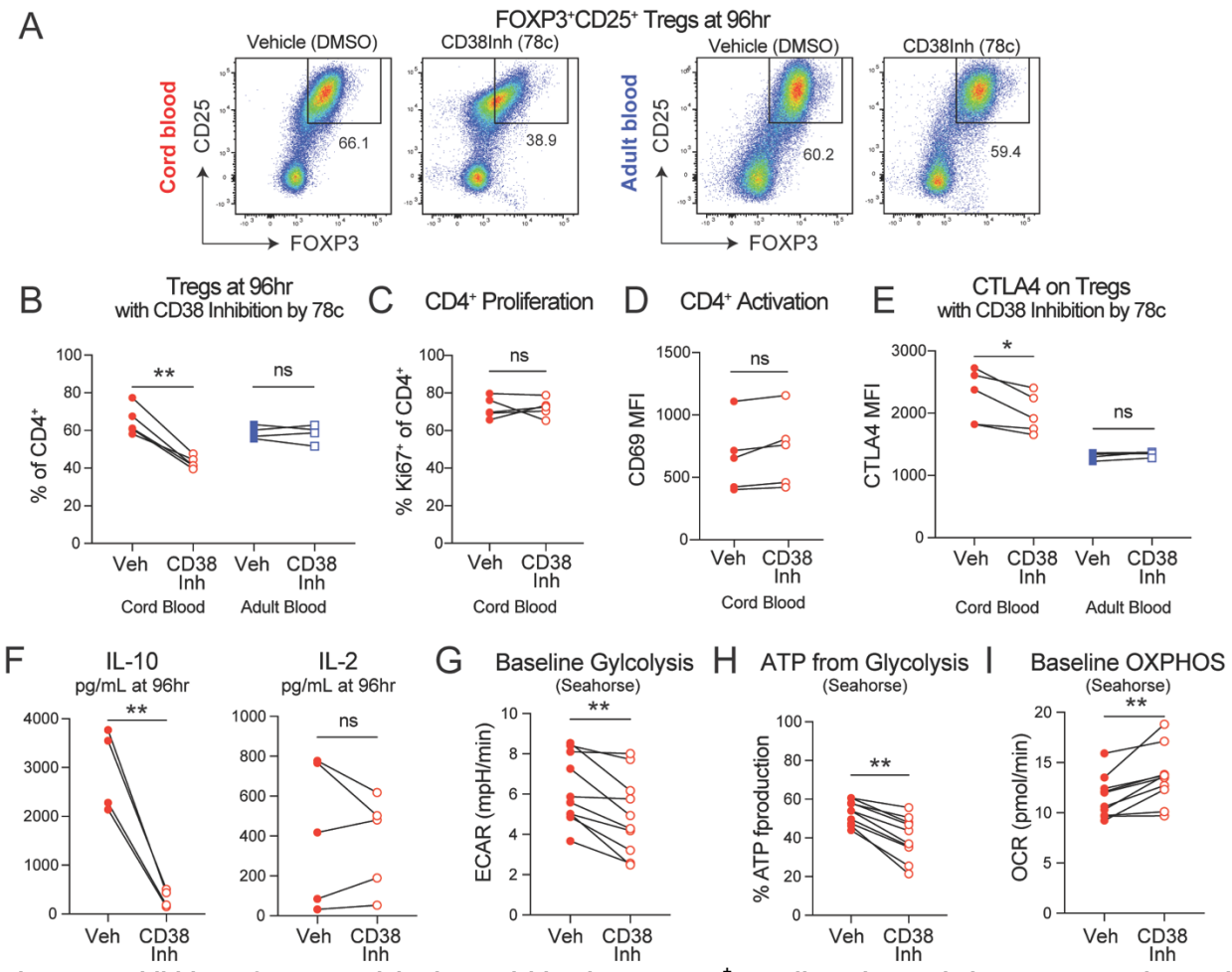

Figure 5: Inhibition of CD38 activity in cord blood naïve CD4$^+$ T cells reduces their Treg generation and glycolytic capacity (A, B) Representative flow plots and graph of the percentage of FOXP3$^+$CD25$^+$ (Tregs) from cord blood (CB) and adult blood (AB) 96hr stimulated cells with vehicle (DMSO) or CD38 inhibitor (5uM 78c). Cells were treated with DMSO or 78c for 24hr prior to activation and Treg measurement 96hr after stimulation. (C, D) CB Tregs proliferation (Ki67) and activation (CD69) were not changed between DMSO and 78c treatment. (E) CTLA4 MFI on Tregs from CB was reduced with CD38 inhibition with no change in CTLA MFI on AB Tregs. (F) ELISA-based measurement of cytokines in cell culture supernatant of DMSO or 78c treated CB stimulated naïve CD4$^+$ T cells at 96hr. (G) Quantification of baseline glycolysis between DMSO and 78c treated CB naive CD4$^+$ T cells via Seahorse. (H) Percent of ATP made from glycolysis for DMSO versus 78c treated CB naive CD4$^+$ T cells via Seahorse. (I) Baseline oxidative phosphorylation of DMSO and 78c treated CB naive CD4$^+$ T cells via Seahorse. All data points represent individual samples from different biological donors. A-E and G-I display one representative experiment from three repeats. F displays one experiment.

We next assessed the contribution of CD38 expression by CB naïve CD4$^+$ T cells on their metabolic state, treating CB and AB cells with 10uM of 78c for 24 hours prior to metabolic assessment via Seahorse. Inhibition of CD38 in CB naive CD4$^+$ T cells resulted in decreased ECAR as well as total ATP made from glycolysis with an accompanying increase in OXPHOS (**Figure 5G-I**). This is consistent with previous studies in adult effector T cells from mice and humans, where genetic deletion or pharmacological inhibition of CD38 resulted in increased OXPHOS and mitochondrial function[18,41]. Notably though, naïve CD4$^+$ T cells from AB did not

show significant changes in their metabolic state at levels of CD38 inhibition sufficient to alter CB cell function (**Figure S5E-G**). Together, these data suggest that CD38 expression contributes to the unique, glycolytically-dependent state of CB naïve $CD4^+$ T cells as well as their Treg potential.

The CD38-NAD-SIRT1 axis controls the distinct Treg fate of neonatal naïve $CD4^+$ T cells

We next sought to further dissect how CD38 might functionally shape the metabolic state and Treg potential of CB naïve $CD4^+$ T cells. CD38's enzymatic function in catalyzing the synthesis of ADP ribose and cADPR has been shown to deplete cellular NAD+ stores[18]. Consistent with this being a relevant mechanism in our studies, we observed lower NAD+ levels in naïve $CD4^+$ T cells from CB as compared to AB (**Figure 6A**). Furthermore, pharmacological inhibition of CD38 in CB naïve $CD4^+$ T cells led to an increase in NAD+ levels **(Figure 6B**). NAD+ can impact cellular function through multiple avenues, including its role as a cofactor for oxidoreductases, an electron donor for redox reactions and a substrate for the sirtuin family of deacetylases [42]. We were particularly intrigued by this third possibility, given existing literature linking the sirtuin family member, SIRT1, to T cell metabolism and FOXP3 expression. Specifically, low SIRT in terminally differentiated human memory $CD8^+$ T cells was shown to facilitate their glycolytic state[43]. Separately, SIRT1-mediated histone deacetylation has been shown to decrease chromatin accessibility of the *FOXP3* locus[44], and SIRT1 deacetylation of FOXP3[29,30] targets the protein for degradation. Thus, in CB, where high CD38 reduces cellular NAD+ levels, we could expect lower SIRT1 activity to enable glycolysis and increase FOXP3 expression (**Figure 6C**).

To test this, we treated CB and AB naïve $CD4^+$ T cells with a SIRT1 Activator (SRT 2104), a SIRT1 Inhibitor (Selisistat), or DMSO as a vehicle control for 24 hours prior to anti-CD3/CD28 activation and Treg measurement 96 hours later. Indeed, SIRT1 activation significantly impeded Treg generation by CB naive $CD4^+$ T cells, with a parallel but lower magnitude reduction seen in AB. However, while SIRT1 inhibition did not impact CB Tregs, it increased AB Treg generation to a level more comparable to CB (**Figure 6D**). This supports the idea that very low SIRT1 activity in CB naïve $CD4^+$ T cells contributes to their increased Treg generation, whereas AB cells have at baseline somewhat higher SIRT1 activity, which can be further modulated pharmacologically to tune their Treg potential.

In other cell types, SIRT1 is known to engage in a negative feedback loop with the nuclear hormone receptor PPARγ[45,46]. PPARγ is a pleiotropic transcription factor best known for its role in adipogenesis, lipid metabolism and insulin sensitivity[47]. It has also been shown to have a key role in the biology of fat-resident Tregs[48] as well as in Treg generation and function more broadly[49–51]. In our RNA-seq dataset, PPARγ gene counts were about 10-fold higher in 48 hour stimulated $CD4^+$ T cells from CB versus AB (**Figure 6E**). To test if increased neonatal PPARγ expression could also contribute to increased early life Treg generation, we treated naïve $CD4^+$ T cells with the PPARγ agonist Rosiglitazone, the PPARγ antagonist GW9662, or DMSO vehicle control for 24 hours prior to activation. Measurement of CB Tregs at 96 hours revealed no change with PPARγ agonism, but PPARγ antagonism did lead to a significant CB Treg reduction. Conversely, AB Tregs were increased to levels commensurate with CB in the presence of Rosiglitazone, with no effect from GW9662 (**Figure 6F-G**). These data suggest that differential age-dependent PPARγ expression in naïve $CD4^+$ T cells contributes to their distinct capacities for Treg generation.

Finally, we sought to clarify if CD38 levels and, by extension, SIRT1-modulation of Treg potential in naïve $CD4^+$ T cells was mediated primarily through regulation of PPARγ. To dissect this, we pre-treated naïve $CD4^+$ T cells prior to activation with our SIRT1 activator, PPARγ agonist, or both. Interestingly, while we again observed reduced CB and AB Tregs with SIRT1 activation alone, addition of Rosiglitazone to agonize PPARγ in this setting only led to a partial restoration of CB Tregs (**Figure 6H**). This result indicates that the CD38-NAD-SIRT1 axis works through multiple different mechanisms to influence the $CD4^+$ T cell-intrinsic capacity for early life Treg generation. While PPARγ may be one key downstream pathway, it is likely that direct effects of SIRT1 on *FOXP3* locus accessibility, FOXP3 protein stability, and possibly the metabolic state of naïve $CD4^+$ T cells are also critical. Together, these studies provide significant new mechanistic insights into how heightened neonatal expression of CD38 in the naïve $CD4^+$ T cell compartment helps enable the early life window for Treg generation and tolerance.

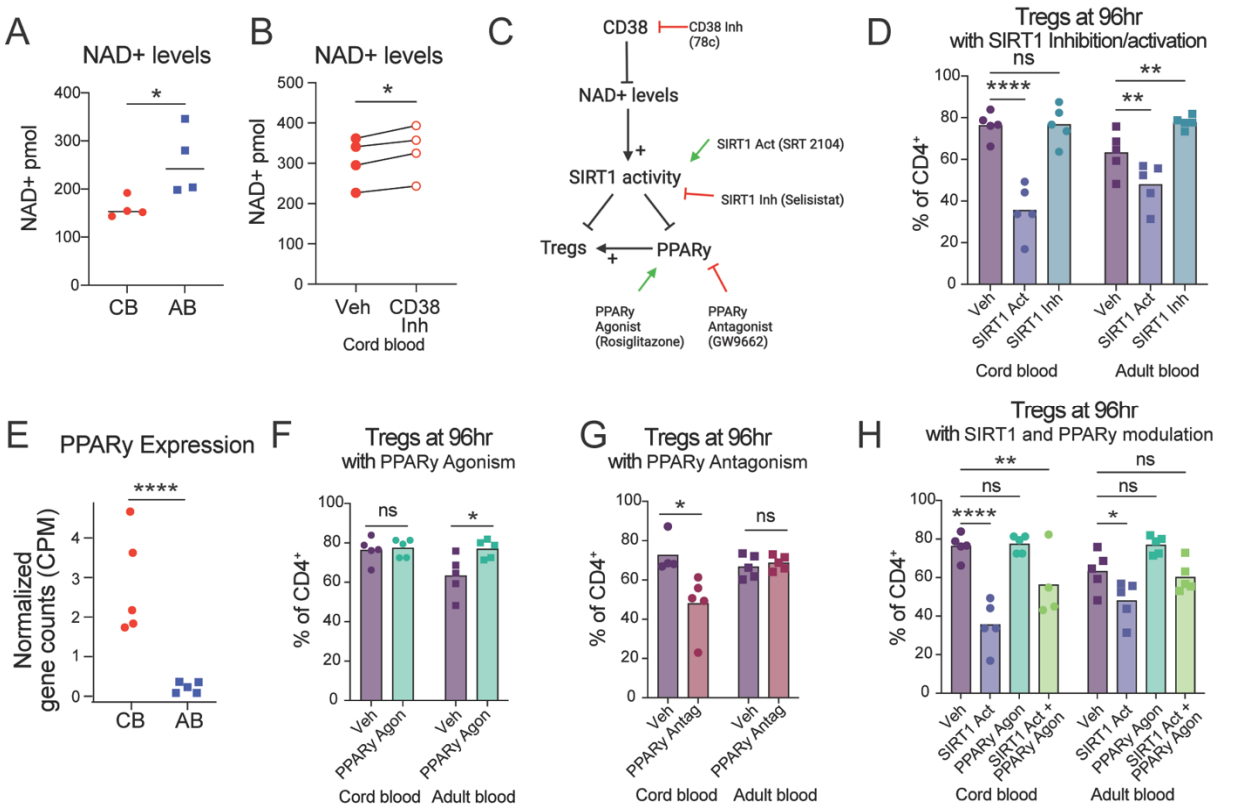

Figure 6: The NAD+ dependent deacetylase, SIRT1, modulates the Treg generation capacity of cord blood naïve CD4$^+$ T cells (A) NAD+ levels measured between cord blood (CB) and adult blood (AB) naïve CD4$^+$ T cells at baseline. (B) NAD+ levels measured between DMSO or 78c 24hr treated CB naïve CD4$^+$ T cells at baseline. (C) Schematic of CD38-NAD-SIRT1-Tregs-PPARy pathway with pharmacological perturbations used in subsequent experiments included. (D) CB and AB naïve CD4$^+$ T cells were treated with vehicle control (DMSO), SIRT1 activator (20uM of SRT 2104), or SIRT1 inhibitor (20uM of Selisistat) for 24 hours prior to activation and Treg measurement 96hr after activation. (E) Normalized gene counts of PPARy (PPARG gene) at 48hr after activation from bulkRNAseq data. (F) CB and AB naïve CD4$^+$ T cells were treated with vehicle control (DMSO) or PPARy agonist (60uM of Rosiglitazone) for 24 hours prior to activation and Treg measurement 96hr after activation. (G) CB and AB naïve CD4$^+$ T cells were treated with vehicle control (DMSO) or PPARy antagonist (2.5uM of GW9662) for 24 hours prior to activation and Treg measurement 96hr after activation. (H) CB and AB naïve CD4$^+$ T cells were treated with vehicle control (DMSO), SIRT1 activator (20uM of SRT 2104), PPARy agonist (60uM of Rosiglitazone), or both SIRT1 activator and PPARy agonist for 24 hours prior to activation and Treg measurement 96hr after activation. All data points represent individual samples from different biological donors. A, B, D, F-G show one experimental replicate of two.

Discussion

Here we demonstrate that early life naïve $CD4^+$ T cells have a unique metabolic state, characterized by a higher reliance on glycolysis, and that this directly impacts their distinct functional potential for Treg generation. We further identify CD38 as a key age-dependent regulator, increased on circulating naïve $CD4^+$ T cells from cord blood and human infants, which modulates both their metabolic state and Treg differentiation capacity. In contrast, the adult naïve $CD4^+$ compartment is characterized by negligible CD38 expression, which corresponds to low glycolytic dependence and Treg potential. Via functional manipulation of CD38's enzymatic function, we demonstrate that its role as an NADase in neonatal $CD4^+$ T cells limits SIRT1 deacetylation, which in turn contributes to increased Tregs, likely via several mechanisms including modulation of PPARγ expression, cell metabolic state, as well as direct tuning of FOXP3 expression. Collectively, this work elucidates a central paradigm governing neonatal generation of Tregs, which functionally enables the early life window of opportunity for establishing peripheral immune tolerance.

These observations open new questions about what regulates CD38 expression on naïve $CD4^+$ T cells, and how it shifts in an age-dependent manner. PAXIP1 (also referred to as Pax-interacting protein 1 or PTIP) has been shown in macrophages to promote CD38 expression by cooperatively increasing H3K27 acetylation of an intronic enhancer[52]. PAXIP1 has not been specifically studied as a regulator of CD38 in T cells but does have established roles in the early stages of T cell development, specifically enabling genomic stability during TCR gene re-arrangement and promoting expression of S1PR1 on single-positive thymocytes to enable their thymic egress[53]. Whereas PAXIP1 is not known to have differential expression by age, the RNA-binding protein, Lin28b, is specifically increased in early life hematopoietic progenitor cells, where it is thought to shape many features of fetal and neonatal lymphocytes[17,54]. Studies in separate cell types have also shown that Lin28 promotes glucose metabolism via its inhibition of the let-7 microRNA and downstream activation of MTOR signaling[55], making it another intriguing candidate for shaping age-dependent CD38 expression.

Very recent work has suggested that CD38 is enriched on recent thymic emigrants (RTEs)[23], which provides an intriguing explanation for why CD38 expression might be increased in the early life window, which is demarcated by high thymic output[56]. However, rather than bimodal expression of CD38 in the neonatal naïve $CD4^+$ compartment, we observe that the mean CD38 expression shifts down with age for the entire population. A slow decrease in CD38 levels

among circulating CD4$^+$ T cells following thymic egress, in tandem with diminishing thymic output could lead to this pattern of expression. However, an age-associated shift in CD38 expression on single positive T cells leaving the thymus remains a separate possibility. Thus, further studies are needed to define key regulators of CD38 expression in T cells and how this relates to the age at which they were generated and the length of time they have spent in circulation.

Beyond CD38 specifically, our work underscores the concept that the metabolic state of early life lymphocytes fundamentally shapes their functional capacity[33,57]. We show that human naïve neonatal CD4$^+$ T cells exhibit higher relative dependence on glycolysis than their adult counterparts, analogous to findings in human CD8$^+$ T cells[58]. Prior work in murine models has linked the glycolytic state of neonatal CD8$^+$ T cells to heightened effector memory differentiation and a reduced capacity for generation of central memory subsets[17]. Here we show that reducing the glycolytic state of CB naïve CD4$^+$ T cells, either directly via 2DG or indirectly via 78c, diminishes their capacity for Treg generation. Further work is needed, however, to decipher the mechanistic basis of this link between naïve CD4$^+$ T cell metabolism and function. One possibility based on the literature[56] is that a high glycolytic state reduces activity of myc-promoted binding protein (MBP1), a transcription factor known to repress of a *FOXP3*-E2 splice variant[59]. Glycolysis-facilitated release of this repression may increase expression of this splice variant previously shown to promote Treg differentiation and stability[60]. However, given the body of work illustrating the importance of OXPHOS in the function of fully differentiated Tregs [61,62], additional work will be needed to disentangle the longer-term fate of Tregs emerging from the neonatal naïve CD4$^+$ T cell compartment. Development of animal models, analogous to those used to study neonatal versus adult CD8$^+$ T cells[39], will hopefully help determine if the glycolytic tone accompanying the induction of Tregs from neonatal CD4$^+$ T cells negatively impacts their stability of function.

We identified SIRT1 as a key downstream regulator of CD38's effects in neonatal naïve CD4$^+$ T cells, illustrating that low SIRT1 activity due to high CD38 NADase function promotes a unique cell metabolic state and functional capacity. While SIRT1 activity is known to increase in aging cells and mediate physiological changes associated with healthy aging, most literature has focused on differential activity between mid and late adult life, with little attention paid thus far to specific repression of its activity in the neonatal window[63]. Given the wide range of histone and non-histone SIRT1 acetylation targets, changes in multiple cell pathways likely contribute to

SIRT modulation of T cell behavior. Thus, disentangling their relative impact in neonatal T cells will take extensive work. Key candidate mechanisms for further study include direct de-repression of FOXP3 at either the gene or protein level[30,64] and augmentation of glycolysis over OXPHOS via key intermediary transcription factors, e.g. PGC-1α, HIF-1α, or enzymes, e.g. PGAM1[65–67]. We also show a potential role for PPARγ as another SIRT1 interactor that could influence both $CD4^+$ T cell metabolism and Treg potential[51,68]. SIRT1 has been shown to inactivate PPARγ via its deacetylation[45]. Thus, low SIRT1 activity in neonatal naïve $CD4^+$ T cells might contribute to higher PPARγ activity and Treg-promoting function. Additionally, PPARγ can inhibit SIRT1 expression at the transcriptional level providing a potential negative feedback loop that could serve as another modulator of SIRT1 activity neonatally in addition to low NAD+ levels[46].

In conclusion, our findings highlight the translational potential of modulating CD38 expression and glycolytic state in neonatal naïve $CD4^+$ T cells to influence Treg generation. By characterizing CD38 as a metabolic regulator within neonatal T cells, we reveal a potential target for therapeutic strategies aimed at enhancing peripheral tolerance in early life, which could be especially relevant for preventing immune disorders linked to insufficient Treg development, such as autoimmunity and allergy. Furthermore, our work underscores the need for age-specific approaches in immune modulation, as metabolic interventions that enhance Treg induction in neonates may differ substantially from those required in adults. The unique neonatal environment, with its distinct metabolic cues and regulatory proteins like CD38, provides an essential opportunity to understand and leverage the age-dependent plasticity of immune cells. Translationally, future studies targeting these pathways could refine interventions in neonatal immune regulation, advancing both preventive and therapeutic strategies for immune tolerance in early life.

Limitations of the study:

Due to constraints in human sample collection, obtaining sufficient quantities of post-natal infant blood proved challenging. Consequently, cord blood was utilized in this study as a surrogate for early life samples. Although we were able to confirm the persistently high expression of CD38 in a limited number of post-natal samples, we were unable to fully validate all findings in these samples. This limitation, coupled with the scarcity of post-natal samples, restricted our capacity to examine graded changes in CD38 expression, metabolic state, and Treg potential within the post-natal period to assess temporal dynamics. Collecting early life (0-18 years) human samples is an ongoing collaborative effort and will form the basis of future studies focused on delineating the timing and progression of these age-related observations.

In this study, we used pharmacological agents rather than genetic approaches to dissect the functional role of CD38 in neonatal $CD4^+$ T cells. This choice was informed by observations that CRISPR electroporation of cord blood naïve CD4+ T cells impaired their activation capacity, even when using a scramble control without CD38 disruption. Moreover, genetic disruption via CRISPR requires cell activation, which would not allow us to assess age-dependent differences in a resting state. Therefore, we opted to use pharmacological compounds that have been well-validated and further optimized the dosing and treatment conditions within our system. Efforts to refine CRISPR techniques for cord blood naïve $CD4^+$ T cells are ongoing to enable genetic manipulation of CD38 and its downstream mediators. Finally, future work is needed to determine whether CD38 expression specifically promotes Treg differentiation in naïve $CD4^+$ T cells or if it contributes more globally to their differentiation into Th1, Th2 and Th17 effector subsets.

Acknowledgements:

We thank Rafael Argüello Ph.D. for contribution of SCENITH reagents, Joanna Halkias M.D., Ph.D., Ari Molofsky M.D., Ph.D., Rachel Rutishauser M.D., Ph.D., Michael Rosenblum M.D., Ph.D. and Qizhi Tang Ph.D. for helpful discussions. Umbilical cord blood units utilized in this project were obtained from the Umbilical Cord Blood Collection Program, made available under the California Health & Safety Code §§ 1627-1630, and maintained by the Institute for Regenerative Cures, University of California at Davis, Sacramento, CA 95817. Infant blood was obtained from a collaboration with the PROMPT/PREMO Cohort with assistance from NIH Grant R01 HD102381-01 and UCSF's Benioff Center for Microbiome Medicine. We acknowledge UCSF's Parnassus Flow CoLab (RRID:SCR_018206) for assistance in flow cytometry and cell

sorting, supported by NIH grant P30 DK063720. We thank Sandler Program for Breakthrough Biomedical Research Technologies, Methodologies & Cores and UCSF NORC grant (P30DK098722) for funding and use of the Seahorse machine for metabolism measurements. L.D. was supported by funds from the UCSF Immunology T32 Training Grant (NIH grant T32AI007334-33), and a Trainee Research Award from UCSF's Benioff Center for Microbiome Medicine. Work was supported by startup funds from UCSF Department of Dermatology.

Author Contributions

L.D. and T.C.S. designed the studies and wrote the manuscript. L.D. performed the experiments and analyzed the data. S.C. performed analysis of bulk RNA-seq data. V.G. assisted in experimental design and execution. C.C. performed COMPASS analyses. E.E.R., S.P.O, and L.L.J.P. provided access to preterm birth samples. S.V.L., A.W. and A.J.C provided resources and input on experimental design. T.C.S. oversaw all study design and data analysis. All authors discussed results and commented on the manuscript.

Declaration of Interests

T.C.S. is on the Scientific Advisory Board of Concerto Biosciences. L.L.J.P and S.P.O. have patents pending for a tool predicting preterm birth and for a newborn metabolic vulnerability model for identifying preterm infants at risk of adverse outcomes. S.V.L is a board member and consultant for Siolta Therapeutics, Inc, and holds stock in the company. She also consults for Sanofi and for the Atria Institute of New York. A.J.C. receives research support from Eli Lilly and Genentech for work unrelated to this manuscript. Other authors have no competing interests.

METHODS

Experimental Model and Subject Details

Human Blood Samples

Deidentified human cord blood samples were purchased University of California, Davis from the California Umbilical Cord Blood Collection Program (UCBCP). Donors were screened for healthy full term birth, normal weight and no commodities in mother or infant. Healthy non-obese, non-smoking adult donors of ages 18-45 were consented for blood donation under IRB Number 12-09489 and IRB Number 13-11307. Infant blood samples were obtained from UCSF participants in the Prediction of Maturity, Morbidity, in Preterm Infants (PROMPT) study. This is a multi-site NIH study funded by the NIH (R01 HD102381-01) with a common IRB (together with the University of Iowa) approved by the Western Institutional Review Board (WCG IRB), IRB number 20202748, and conducted in accordance with all applicable ethical guideline and regulations for human subject research. Infant peripheral blood samples were taken from 4 preterm infants at 6 weeks of age. Cord blood samples were shipped overnight, and adult and infant blood samples were obtained, left on a rocker at room temperature, and processed within 12 hours of collection. All samples were then uniformly processed using a Ficoll-Plaque gradient to isolate peripheral blood mononuclear cells (PBMCs). PBMCs were frozen at a concentration of 10mil/1mL in freezing media (90% FBS, 10% DMSO) and were then stored in a liquid nitrogen tank. Sample collection was attentive in considering sex as a biological variable and included equal proportions of cord blood and adult blood samples from male and female donors.

Method Details

Cell Culture and Stimulation

Cells were thawed and washed before resting overnight in a 37C 5% CO2 incubator in Resting Media (RPMI with 10% FBS, 1% 100x Pen/Strep, 1% Hepes, and 1% Glutamax). After resting, naïve $CD4^+$ T cells were isolated using the StemCell EasySep™ Human Naïve $CD4^+$ T Cell Isolation Kit. For stimulation assays on which RNA sequencing was performed (see details below), live naïve $CD4^+$ T cells were isolated by fluorescence-activated cell sorting (FACS) based on the following markers: $CD4^+CD8^-CD45RA^+CD27^+CCR7^+CD95^-$. Naïve $CD4^+$ T cells were either used immediately or activated and cultured with STEMCELL ImmunoCult™ Human CD3/CD28 T Cell Activator in STEMCELL Immunocult™ T cell Media (+ 0.1% Pen/Strep) at a concentration of 100,000 cells/200uL media in 96 well U bottom plates in a 37C 5% CO2 incubator for up to 96 hours post-activation. No cytokines were added to the culture. To verify appropriate activation, ImmunoCult™ Human CD3/CD28 T Cell Activator was compared to other

standardized protocols for human T cell activation: Dynabeads™ Human T-Activator CD3/CD28 for T Cell Expansion and Activation, coating the plate in 2ug/mL CD3 and 4ug/mL CD28 antibodies either overnight at 4C or for 4 hours at 37C before washing and adding cells for activation.

ELISA: Supernatants from cell culture were taken at the time of staining for flow cytometry. 120uL of supernatant for each sample were stored at -80C and sent to Eve Technologies for analysis using their "Human Cytokine Proinflammatory Focused 15-Plex Discovery Assay® Array (HDF15)."

SCENITH: SCENITH was performed as described previously[40]. SCENITH reagents (inhibitors, puromycin, anti-puromycin antibodies) were obtained from Rafael Argüello Ph.D. and used according to kit instructions for in vitro human T cell metabolic profiling. Briefly, 100,000 non-activated naïve $CD4^+$ T cells or 96 hour activated cells were incubated for 20 minutes with Control (DMSO), 2-Deoxy-Glucose (2DG; 100 mM), Oligomycin (O; 1 µM), or a combination of 2DG and Oligomycin (DGO). Following incubation with inhibitors, Puromycin (final concentration 10 µg/mL) was added to the culture. Due to their lower metabolic state, non-activated cells were incubated with Puromycin for 40 minutes, while 96 hour activated cells were incubated for 15 minutes. After puromycin treatment, cells were washed with cold PBS and stained for flow cytometry in a panel that included an anti-puromycin antibody. Changes in puromycin MFI between conditions were used as a readout for changes in metabolic state when inhibitors of pathways were added.

Seahorse: Cells were analyzed using an Agilent Seahorse XFe96 analyzer with the Seahorse XF T Cell Metabolic Profiling Kit. Naïve $CD4^+$ T cells were seeded at 150,000 cells/well and kit protocol was followed. Results were analyzed using the Agilent Seahorse Analytics web browser.

Antibody Staining of Immune Cells: Cells were stained for surface antibodies in PBS + 10% FBS for 30 minutes at 4C. For intracellular staining, cells were fixed and permeabilized using the Foxp3 staining kit (eBioscience, Catalog No. 00-5523-00) buffer for 20 minutes at 4ºC then stained in permeabilization buffer for 60 minutes at 4ºC.

Flow cytometry: Stained cells were run on a Fortessa (BD Biosciences) in the UCSF Flow Cytometry Core. Flow cytometry data was analyzed using FlowJo software (FlowJo, LLC).

Pharmacological Perturbations: Chemicals were added after naïve $CD4^+$ T cell isolation. Cells were rested for 24 hours with chemicals and were analyzed via Seahorse for non-activated metabolic impacts or were activated with ImmunoCult™ Human CD3/CD28 T Cell Activator and stained for flow cytometric analysis 96 hours after activation. The following chemicals were used: 2-Deoxy-Glucose (2DG; 0.5mM), CD38 inhibitor 78c (Sigma-Aldrich Cat #5387630001), final concentration 5uM; Selisistat (EX 527, SEN0014196) SIRT1 inhibitor, final concentration 20uM; SRT 2104 activator of Sirt1, final concentration 20uM; Rosiglitazone (BRL 49653) a selective PPARγ agonist, final concentration 60uM; GW9662, PPARy antagonist, final concentration 2.5uM.

NAD+ Levels: Naïve $CD4^+$ T cells were isolated and the NAD/NADH Assay Kit (Colorimetric) (Abcam Cat # ab65348) was used according to the manufacturer's protocol.

Statistics: Unless otherwise noted, statistics throughout figures reflect unpaired or paired t-tests (noted by linked data points), with Bonferroni adjustment for multiple comparison; p values for RNAseq data are adjusted for false discovery rate, with resulting p-values: * ≤ 0.05, ** ≤ 0.02, *** ≤ 0.001, **** < 0.0001.

Generation of Bulk RNA-seq Data:

Naïve $CD4^+$ T cells ($CD4^+CD8^{neg}CD45RA^+CD27^+CCR7^+CD95^{neg}$) were isolated by FACS from CB and AB samples. For baseline (non-activated) cells, 1 million naïve $CD4^+$ T cells were washed with PBS, pelleted in an Eppendorf tube, and frozen at -80C to lyse and store cells. For the other time points, 1 million sorted naïve cells were seeded in a 96-well plate at a density of 100,000 cells/well and cultured at 37C with Immunocult™ anti-CD3/CD28 soluble antibodies. Cultures were harvested at 3hr, 24hr, or 48hr post-activation and processed the same as the baseline time point. Frozen cell pellets were shipped to Novogene on dry ice, where sample quality control, library construction, and sequencing occurred according to their standard protocol[69]. Messenger RNA was purified from total RNA using poly-T oligo-attached magnetic beads. After fragmentation, the first strand cDNA was synthesized using random hexamer primers, followed by the second strand cDNA synthesis using either dUTP for directional library or DTTP for non-directional library. For the non-directional library, it was ready after end repair,

A-tailing, adapter ligation, size selection, amplification, and purification. For the directional library, it was ready after end repair, A-tailing, adapter ligation, size selection, USER enzyme digestion, amplification, and purification. The library was checked with Qubit and real-time PCR for quantification and bioanalyzer for size distribution detection. Quantified libraries were pooled and sequenced on Illumina Novaseq 6000, S4 Flowcell, Paired-End 150 cycles. Samples that passed QC were advanced to RNA sequencing and included in data analysis. Six samples for each age and time point were submitted, but only those that passed RNA quality control were advanced to sequencing and analysis. The final number of individual samples from different donors for each time point are as follows: 0HR: 6CB, 5AB; 3HR: 5CB, 5AB; 24HR: 5CB, 5AB; 48HR: 5CB, 5AB.

Bulk RNA-seq Analysis

Processing

cDNA and ncRNA fasta files from Ensembl GRCh38 (version 109)[70] were concatenated and used as input to the kallisto (0.46.2)[71] `index` function with default arguments. The kallisto `quant` function was used to perform paired-end transcript quantification. The transcript-level estimates from kallisto were imported into R (version 4.4.1)[72] and summarized to gene estimates using the tximport (1.32.0)[73] package (`type = “kallisto”, countsFromAbundance = “lengthScaledTPM”, ignoreTxVersion = TRUE`) from Bioconductor (version 3.19)[74]. Ensembl IDs were mapped to gene symbols using the `makeTxDbFromEnsembl` function from the txdbmaker (1.0.1)[75] and biomaRt packages[76] (2.60.1) using version 109 of the `hsapiens_gene_ensembl` dataset. Genes with scaffold and haplotype chromosome annotations were removed prior to downstream analysis.

These gene counts were then used to create a `DEGList` object, followed by filtering on lowly expressed genes using the function `filterByExprs` with the group argument set to the interaction of sample age (cord blood (CB), adult blood (AB)) and time point (0, 3, 24, 48 hours) using the edgeR (4.2.2) package[77]. Normalization factors were generated using the trimmed mean of M-values (`TMM`) method[78]. The `cpm` function from edgeR with a prior count of 3 was used to generate normalized log2 counts per million (CPM) as input for principal component analysis (PCA) and heatmaps after regressing on the effect of sex using the `removeBatchEffect` function from the limma (3.60.6)[79]. Gene count plots were generated with

CPM values without log transformation. PCA was performed using the `prcomp` function from the R stats package (4.4.1) with `scale = TRUE` on the 500 most variable genes, as in the `plotPCA` function from DESeq2 (1.44.0)[80]. Heatmaps were generated using 2,000 features with the highest row variances after excluding T cell receptor variable and major histocompatibility complex associated genes. Row transformation and ordering of the heatmaps was performed using the `coolmap` function from limma with the argument `cluster.by = "de pattern"`. The `cuttree` function from the R stats package was used to identify hierarchical clusters of genes with `k = 8` clusters. Mean gene z-scores were used to summarize moving expression averages of the clusters across time points.

Differential Expression of bulk RNA-seq

Differential gene expression and summary gene statistics were analyzed using linear models (`lmFit`) with empirical Bayes moderation (`eBayes`) and observational weighting (`voomWithQualityWeights`) with the limma package[81,82]. A null intercept model accounting for group (interaction of age and time point) and sex was used for the `design` argument. Adjusted p-values were obtained using the Benjamini-Hochberg correction using the `topTable` function from limma. Statistical significance was determined based on a log2 fold change threshold of 0.585 and a Benjamini-Hochberg adjusted p-value threshold of 0.05.

Gene set Enrichment

Gene Ontology Biological Processes (GO:BP) pathways were obtained from the ontology gene set collection (C5) from the Molecular Signatures Database (MSigDB)[83,84]. Gene Set Enrichment Analysis (GSEA) was performed using the fgsea package (1.30.0) with `scoreType = “std” `[37,38]. Gene enrichment statistics were ranked by descending log2 fold change and genesets were required to contain at least 15 unique genes (`minSize = 15).

Analysis of scRNA-seq data:

Raw counts were first normalized to total counts of 1e4 and log-transformed. Then, differential expression was performed using a Wilcoxon rank-sum test provided by the sc.pp.rank_genes_groups method in the scanpy package (version 1.9.4)[85]. Genes with log-fold change > 4 or < -4 were shifted to 4 and -4 respectively for display purposes in Figure 2E. Metabolic genes were curated from the Human1 GEM[86].

Compass analysis:

Pseudobulking was performed on the scRNA-seq dataset by averaging gene expression profiles of single cells that belonged to the same donor (n=5 for CB and AB groups Module-Compass[27] was performed on central carbon pathways (glycolysis, TCA, and OXPHOS) reactions curated from the Human1 GEM[86]. Raw reaction scores were negative transformed and shifted as described in [Compass reference]. Variance shrinkage and linear modeling of transformed reaction scores with condition as the independent variable were performed using the limma package[79].

Data Availability and Software Used

- Schematics were made with Biorender (https://biorender.com). GraphPad (Prism) 10 was used. R version 4.4.1 was used for bulk and single cell RNA-seq analyses.
- The bulk RNA-seq data generated in this study has been deposited to the GEO as indicated in the key resources table.
- Any additional information required to reanalyze the data reported in this paper is available from the lead contact upon request.

References

1. Gensollen, T., and Blumberg, R.S. (2017). Correlation between early-life regulation of the immune system by microbiota and allergy development. Journal of Allergy and Clinical Immunology *139*, 1084–1091. https://doi.org/10.1016/J.JACI.2017.02.011.

2. Yang, S., Fujikado, N., Kolodin, D., Benoist, C., and Mathis, D. (2015). Immune tolerance. Regulatory T cells generated early in life play a distinct role in maintaining self-tolerance. Science *348*, 589–594. https://doi.org/10.1126/SCIENCE.AAA7017.

3. Suri-Payer, E., Amar, A.Z., Thornton, A.M., and Shevach, E.M. (1998). CD4+CD25+ T cells inhibit both the induction and effector function of autoreactive T cells and represent a unique lineage of immunoregulatory cells. J Immunol *160*, 1212–1218. https://doi.org/10.4049/jimmunol.160.3.1212.

4. Asano, M., Toda, M., Sakaguchi, N., and Sakaguchi, S. (1996). Autoimmune disease as a consequence of developmental abnormality of a T cell subpopulation. J Exp Med *184*, 387 – 396.

5. Wang, G., Miyahara, Y., Guo, Z., Khattar, M., Stepkowski, S.M., and Chen, W. (2010). “Default” generation of neonatal regulatory T cells. J Immunol *185*, 71–78. https://doi.org/10.4049/JIMMUNOL.0903806.

6. Mold, J.E., Venkatasubrahmanyam, S., Burt, T.D., Michaëlsson, J., Rivera, J.M., Galkina, S.A., Weinberg, K., Stoddart, C.A., and McCune, J.M. (2010). Fetal and Adult Hematopoietic Stem Cells Give Rise to Distinct T Cell Lineages in Humans. Science (1979) *330*, 1695–1699. https://doi.org/10.1126/SCIENCE.1196509.

7. Scharschmidt, T.C., Vasquez, K.S., Truong, H.-A., Gearty, S. V, Pauli, M.L., Nosbaum, A., Gratz, I.K., Otto, M., Moon, J.J., Liese, J., et al. (2015). A wave of regulatory T cells into neonatal skin mediates tolerance to commensal microbes. Immunity *43*.

8. Akagbosu, B., Tayyebi, Z., Shibu, G., Paucar Iza, Y.A., Deep, D., Parisotto, Y.F., Fisher, L., Pasolli, H.A., Thevin, V., Elmentaite, R., et al. (2022). Novel antigen-presenting cell imparts Treg-dependent tolerance to gut microbiota. Nature *610*, 752–760. https://doi.org/10.1038/S41586-022-05309-5.

9. Mold, J.E., and McCune, J.M. (2012). Immunological tolerance during fetal development: from mouse to man. Adv Immunol *115*, 73 – 111. https://doi.org/10.1016/b978-0-12-394299-9.00003-5.

10. Ng, M.S.F., Roth, T.L., Mendoza, V.F., Marson, A., and Burt, T.D. (2019). Helios enhances the preferential differentiation of human fetal CD4+ naïve T cells into regulatory T cells. Sci Immunol *4*. https://doi.org/10.1126/SCIIMMUNOL.AAV5947.

11. Bunis, D.G., Bronevetsky, Y., Krow-Lucal, E., Bhakta, N.R., Kim, C.C., Nerella, S., Jones, N., Mendoza, V.F., Bryson, Y.J., Gern, J.E., et al. (2021). Single-Cell Mapping of Progressive Fetal-to-Adult Transition in Human Naive T Cells. Cell Rep *34*. https://doi.org/10.1016/J.CELREP.2020.108573.

12. Anderson, K.A., Madsen, A.S., Olsen, C.A., and Hirschey, M.D. (2017). Metabolic control by sirtuins and other enzymes that sense NAD+, NADH, or their ratio. Biochimica et Biophysica Acta (BBA) - Bioenergetics *1858*, 991–998. https://doi.org/10.1016/J.BBABIO.2017.09.005.

13. Wu, H., Huang, H., and Zhao, Y. (2023). Interplay between metabolic reprogramming and post-translational modifications: from glycolysis to lactylation. Front Immunol *14*. https://doi.org/10.3389/FIMMU.2023.1211221.

14. Holm, S.R., Jenkins, B.J., Cronin, J.G., Jones, N., and Thornton, C.A. (2021). A role for metabolism in determining neonatal immune function. Pediatric Allergy and Immunology *32*, 1616–1628. https://doi.org/10.1111/PAI.13583.

15. Pearce, E.L. (2010). Metabolism in T cell activation and differentiation. Curr Opin Immunol *22*, 314. https://doi.org/10.1016/J.COI.2010.01.018.

16. Chapman, N.M., Boothby, M.R., and Chi, H. (2019). Metabolic coordination of T cell quiescence and activation. Nature Reviews Immunology 2019 20:1 *20*, 55–70. https://doi.org/10.1038/s41577-019-0203-y.

17. Tabilas, C., Wang, J., Liu, X., Locasale, J.W., Smith, N.L., and Rudd, B.D. (2019). Cutting Edge: Elevated Glycolytic Metabolism Limits the Formation of Memory CD8+ T Cells in Early Life. The Journal of Immunology *203*, 2571–2576. https://doi.org/10.4049/JIMMUNOL.1900426.

18. Ghosh, A., Khanam, A., Ray, K., Mathur, P., Subramanian, A., Poonia, B., and Kottilil, S. (2023). CD38: an ecto-enzyme with functional diversity in T cells. Front Immunol *14*, 1146791. https://doi.org/10.3389/FIMMU.2023.1146791.

19. Kar, A., Mehrotra, S., and Chatterjee, S. (2020). CD38: T Cell Immuno-Metabolic Modulator. Cells 2020, Vol. 9, Page 1716 *9*, 1716. https://doi.org/10.3390/CELLS9071716.

20. DeRogatis, J.M., Neubert, E.N., Viramontes, K.M., Henriquez, M.L., Nicholas, D.A., and Tinoco, R. (2023). Cell-Intrinsic CD38 Expression Sustains Exhausted CD8+ T Cells by Regulating Their Survival and Metabolism during Chronic Viral Infection. J Virol *97*. https://doi.org/10.1128/JVI.00225-23.

21. Chatterjee, S., Daenthanasanmak, A., Chakraborty, P., Wyatt, M.W., Dhar, P., Selvam, S.P., Fu, J., Zhang, J., Nguyen, H., Kang, I., et al. (2018). CD38-NAD + Axis Regulates Immunotherapeutic Anti-Tumor T Cell Response. Cell Metab *27*, 85-100.e8. https://doi.org/10.1016/J.CMET.2017.10.006/ATTACHMENT/085FD262-CFBA-4054-B132-E23D1F4E88CC/MMC2.PDF.

22. Reolo, M.J.Y., Otsuka, M., Seow, J.J.W., Lee, J., Lee, Y.H., Nguyen, P.H.D., Lim, C.J., Wasser, M., Chua, C., Lim, T.K.H., et al. (2023). CD38 marks the exhausted CD8+ tissue-resident memory T cells in hepatocellular carcinoma. Front Immunol *14*. https://doi.org/10.3389/FIMMU.2023.1182016.

23. Bohacova, P., Terekhova, M., Tsurinov, P., Mullins, R., Husarcikova, K., Shchukina, I., Antonova, A.U., Echalar, B., Kossl, J., Saidu, A., et al. (2024). Multidimensional profiling of human T cells reveals high CD38 expression, marking recent thymic emigrants and age-related naive T cell remodeling. Immunity *57*, 2362–2379. https://doi.org/10.1016/J.IMMUNI.2024.08.019.

24. Piedra-Quintero, Z.L., Wilson, Z., Nava, P., and Guerau-de-Arellano, M. (2020). CD38: An Immunomodulatory Molecule in Inflammation and Autoimmunity. Front Immunol *11*, 597959. https://doi.org/10.3389/FIMMU.2020.597959.

25. Wei, W., Graeff, R., and Yue, J. (2014). Roles and mechanisms of the CD38/cyclic adenosine diphosphate ribose/Ca2+ signaling pathway. World J Biol Chem *5*, 58. https://doi.org/10.4331/WJBC.V5.I1.58.

26. Cho, Y.S., Han, M.K., Choi, Y.B., Yun, Y., Shin, J., and Kim, U.H. (2000). Direct interaction of the CD38 cytoplasmic tail and the Lck SH2 domain. Cd38 transduces T cell activation signals through associated Lck. J Biol Chem *275*, 1685–1690. https://doi.org/10.1074/JBC.275.3.1685.

27. Wagner, A., Wang, C., Fessler, J., DeTomaso, D., Avila-Pacheco, J., Kaminski, J., Zaghouani, S., Christian, E., Thakore, P., Schellhaass, B., et al. (2021). Metabolic modeling of single Th17 cells reveals regulators of autoimmunity. Cell *184*, 4168-4185.e21. https://doi.org/10.1016/J.CELL.2021.05.045.

28. Li, W., Liang, L., Liao, Q., Li, Y., and Zhou, Y. (2022). CD38: An important regulator of T cell function. Biomedicine and Pharmacotherapy *153*. https://doi.org/10.1016/J.BIOPHA.2022.113395.

29. Van Loosdregt, J., Vercoulen, Y., Guichelaar, T., Gent, Y.Y.J., Beekman, J.M., Van Beekum, O., Brenkman, A.B., Hijnen, D.J., Mutis, T., Kalkhoven, E., et al. (2010). Regulation of Treg functionality by acetylation-mediated Foxp3 protein stabilization. Blood *115*, 965–974. https://doi.org/10.1182/BLOOD-2009-02-207118.

30. Loosdregt, J. van, Brunen, D., Fleskens, V., Pals, C.E.G.M., Lam, E.W.F., and Coffer, P.J. (2011). Rapid Temporal Control of Foxp3 Protein Degradation by Sirtuin-1. PLoS One *6*, e19047. https://doi.org/10.1371/JOURNAL.PONE.0019047.

31. Sequeira, J., Boily, G., Bazinet, S., Saliba, S., He, X., Jardine, K., Kennedy, C., Staines, W., Rousseaux, C., Mueller, R., et al. (2008). sirt1-null mice develop an autoimmune-like condition. Exp Cell Res *314*, 3069–3074. https://doi.org/10.1016/J.YEXCR.2008.07.011.

32. Zhang, J., Lee, S.M., Shannon, S., Gao, B., Chen, W., Chen, A., Divekar, R., McBurney, M.W., Braley-Mullen, H., Zaghouani, H., et al. (2009). The type III histone deacetylase Sirt1 is essential for maintenance of T cell tolerance in mice. J Clin Invest *119*, 3048. https://doi.org/10.1172/JCI38902.

33. Rudd, B.D. (2020). Neonatal T Cells: A Reinterpretation. Annu Rev Immunol *38*, 229–247. https://doi.org/10.1146/ANNUREV-IMMUNOL-091319-083608.

34. Wang, J., Ioan-Facsinay, A., van der Voort, E.I.H., Huizinga, T.W.J., and Toes, R.E.M. (2007). Transient expression of FOXP3 in human activated nonregulatory CD4+ T cells. Eur J Immunol *37*, 129–138. https://doi.org/10.1002/EJI.200636435.

35. Schilham, M.W., Moerer, P., Cumano, A., and Clevers, H.C. (1997). Sox-4 facilitates thymocyte differentiation. Eur J Immunol *27*, 1292–1295. https://doi.org/10.1002/EJI.1830270534.

36. Yu, Y., Wang, J., Khaled, W., Burke, S., Li, P., Chen, X., Yang, W., Jenkins, N.A., Copeland, N.G., Zhang, S., et al. (2012). Bcl11a is essential for lymphoid development and negatively regulates p53. J Exp Med *209*, 2467. https://doi.org/10.1084/JEM.20121846.

37. Korotkevich, G., Sukhov, V., Budin, N., Shpak, B., Artyomov, M.N., and Sergushichev, A. (2021). Fast gene set enrichment analysis. bioRxiv, 060012. https://doi.org/10.1101/060012.

38. Subramanian, A., Tamayo, P., Mootha, V.K., Mukherjee, S., Ebert, B.L., Gillette, M.A., Paulovich, A., Pomeroy, S.L., Golub, T.R., Lander, E.S., et al. (2005). Gene set enrichment analysis: a knowledge-based approach for interpreting genome-wide expression profiles. Proc Natl Acad Sci U S A *102*, 15545–15550. https://doi.org/10.1073/PNAS.0506580102.

39. Tabilas, C., Smith, N.L., and Rudd, B.D. (2023). Shaping immunity for life: Layered development of CD8+ T cells. Immunol Rev *315*, 108–125. https://doi.org/10.1111/IMR.13185.

40. Argüello, R.J., Combes, A.J., Char, R., Gigan, J.-P., Baaziz, A.I., Bousiquot, E., Camosseto, V., Samad, B., Tsui, J., Yan, P., et al. (2020). SCENITH: A Flow Cytometry-

Based Method to Functionally Profile Energy Metabolism with Single-Cell Resolution. Cell Metab *32*, 1063-1075.e7. https://doi.org/10.1016/j.cmet.2020.11.007.

41. Chatterjee, S., Daenthanasanmak, A., Chakraborty, P., Wyatt, M.W., Dhar, P., Selvam, S.P., Fu, J., Zhang, J., Nguyen, H., Kang, I., et al. (2018). CD38-NAD+Axis Regulates Immunotherapeutic Anti-Tumor T Cell Response. Cell Metab *27*, 85-100.e8. https://doi.org/10.1016/J.CMET.2017.10.006.

42. Fang, J., Chen, W., Hou, P., Liu, Z., Zuo, M., Liu, S., Feng, C., Han, Y., Li, P., Shi, Y., et al. (2023). NAD+ metabolism-based immunoregulation and therapeutic potential. Cell & Bioscience 2023 13:1 *13*, 1–15. https://doi.org/10.1186/S13578-023-01031-5.

43. Jeng, M.Y., Hull, P.A., Fei, M., Kwon, H.-S., Tsou, C.-L., Kasler, H., Ng, C.-P., Gordon, D.E., Johnson, J., Krogan, N., et al. (2018). Metabolic reprogramming of human CD8+ memory T cells through loss of SIRT1. J Exp Med *215*, 51. https://doi.org/10.1084/JEM.20161066.

44. Zhang, X., Xiao, X., Lan, P., Li, J., Dou, Y., Chen, W., Ishii, N., Chen, S., Xia, B., Chen, K., et al. (2018). OX40 Costimulation Inhibits Foxp3 Expression and Treg Induction via BATF3-Dependent and Independent Mechanisms. Cell Rep *24*, 607–618. https://doi.org/10.1016/J.CELREP.2018.06.052.

45. Mayoral, R., Osborn, O., McNelis, J., Johnson, A.M., Oh, D.Y., Izquierdo, C.L., Chung, H., Li, P., Traves, P.G., Bandyopadhyay, G., et al. (2015). Adipocyte SIRT1 knockout promotes PPARγ activity, adipogenesis and insulin sensitivity in chronic-HFD and obesity. Mol Metab *4*, 378–391. https://doi.org/10.1016/J.MOLMET.2015.02.007.

46. Han, L., Zhou, R., Niu, J., McNutt, M.A., Wang, P., and Tong, T. (2010). SIRT1 is regulated by a PPARγ–SIRT1 negative feedback loop associated with senescence. Nucleic Acids Res *38*, 7458. https://doi.org/10.1093/NAR/GKQ609.

47. Lehrke, M., and Lazar, M.A. (2005). The many faces of PPARγ. Cell *123*, 993–999. https://doi.org/10.1016/J.CELL.2005.11.026/ASSET/75EFF205-2B62-4C1D-A347-BA858A6E027B/MAIN.ASSETS/GR1.JPG.

48. Cipolletta, D., Feuerer, M., Li, A., Kamei, N., Lee, J., Shoelson, S.E., Benoist, C., and Mathis, D. (2012). PPARγ is a major driver of the accumulation and phenotype of adipose-tissue Treg cells. Nature *486*, 549. https://doi.org/10.1038/NATURE11132.

49. Hontecillas, R., and Bassaganya-Riera, J. (2007). Peroxisome Proliferator-Activated Receptor γ Is Required for Regulatory CD4+ T Cell-Mediated Protection against Colitis. The Journal of Immunology *178*, 2940–2949. https://doi.org/10.4049/JIMMUNOL.178.5.2940.

50. Guri, A.J., Mohapatra, S.K., Horne, W.T., Hontecillas, R., and Bassaganya-Riera, J. (2010). The role of T cell PPAR gamma in mice with experimental inflammatory bowel disease. BMC Gastroenterol *10*. https://doi.org/10.1186/1471-230X-10-60.

51. Wohlfert, E.A., Nichols, F.C., Nevius, E., and Clark, R.B. (2007). Peroxisome Proliferator-Activated Receptor γ (PPARγ) and Immunoregulation: Enhancement of Regulatory T Cells through PPARγ-Dependent and -Independent Mechanisms. The Journal of Immunology *178*, 4129–4135. https://doi.org/10.4049/JIMMUNOL.178.7.4129.

52. Wang, Q., Hu, J., Han, G., Wang, P., Li, S., Chang, J., Gao, K., Yin, R., Li, Y., Zhang, T., et al. (2022). PTIP governs NAD+ metabolism by regulating CD38 expression to drive macrophage inflammation. Cell Rep *38*. https://doi.org/10.1016/J.CELREP.2022.110603.

53. Callen, E., Faryabi, R.B., Luckey, M., Hao, B., Daniel, J.A., Yang, W., Sun, H.W., Dressler, G., Peng, W., Chi, H., et al. (2012). The DNA damage- and transcription-

associated protein paxip1 controls thymocyte development and emigration. Immunity *37*, 971–985. https://doi.org/10.1016/J.IMMUNI.2012.10.007.

54. Dong, M., Mallet Gauthier, È., Fournier, M., and Melichar, H.J. (2022). Developing the right tools for the job: Lin28 regulation of early life T-cell development and function. FEBS J *289*, 4416–4429. https://doi.org/10.1111/FEBS.16045.

55. Zhu, H., Ng, S.C., Segr, A. V., Shinoda, G., Shah, S.P., Einhorn, W.S., Takeuchi, A., Engreitz, J.M., Hagan, J.P., Kharas, M.G., et al. (2011). The Lin28/let-7 axis regulates glucose metabolism. Cell *147*, 81–94. https://doi.org/10.1016/J.CELL.2011.08.033.

56. Murray, J.M., Kaufmann, G.R., Hodgkin, P.D., Lewin, S.R., Kelleher, A.D., Davenport, M.P., and Zaunders, J.J. (2003). Naive T cells are maintained by thymic output in early ages but by proliferation without phenotypic change after age twenty. Immunol Cell Biol *81*, 487–495. https://doi.org/10.1046/J.1440-1711.2003.01191.X.

57. Holm, S.R., Jenkins, B.J., Cronin, J.G., Jones, N., and Thornton, C.A. (2021). A role for metabolism in determining neonatal immune function. Pediatric Allergy and Immunology *32*, 1616–1628. https://doi.org/10.1111/PAI.13583.

58. Sánchez-Villanueva, J.A., Rodríguez-Jorge, O., Ramírez-Pliego, O., Salgado, G.R., Abou-Jaoudé, W., Hernandez, C., Naldi, A., Thieffry, D., and Santana, M.A. (2019). Contribution of ROS and metabolic status to neonatal and adult CD8+ T cell activation. PLoS One *14*, e0226388. https://doi.org/10.1371/JOURNAL.PONE.0226388.

59. De Rosa, V., Galgani, M., Porcellini, A., Colamatteo, A., Santopaolo, M., Zuchegna, C., Romano, A., De Simone, S., Procaccini, C., La Rocca, C., et al. (2015). Glycolysis controls the induction of human regulatory T cells by modulating the expression of FOXP3 exon 2 splicing variants. Nature Immunology 2015 16:11 *16*, 1174–1184. https://doi.org/10.1038/ni.3269.

60. Du, J., Wang, Q., Yang, S., Chen, S., Fu, Y., Spath, S., Domeier, P., Hagin, D., Anover-Sombke, S., Haouili, M., et al. (2022). FOXP3 exon 2 controls Treg stability and autoimmunity. Sci Immunol *7*. https://doi.org/10.1126/SCIIMMUNOL.ABO5407.

61. Kempkes, R.W.M., Joosten, I., Koenen, H.J.P.M., and He, X. (2019). Metabolic Pathways Involved in Regulatory T Cell Functionality. Front Immunol *10*, 483290. https://doi.org/10.3389/FIMMU.2019.02839.

62. Tomaszewicz, M., Ronowska, A., Zieliński, M., Jankowska-Kulawy, A., and Trzonkowski, P. (2023). T regulatory cells metabolism: The influence on functional properties and treatment potential. Front Immunol *14*, 1122063. https://doi.org/10.3389/FIMMU.2023.1122063/BIBTEX.

63. Rogina, B., and Tissenbaum, H.A. (2024). SIRT1, resveratrol and aging. Front Genet *15*, 1393181. https://doi.org/10.3389/FGENE.2024.1393181/BIBTEX.

64. Lu, J., Liang, Y., Meng, H., Zhang, A., Zhao, J., and Zhang, C. (2021). Metabolic Controls on Epigenetic Reprogramming in Regulatory T Cells. Front Immunol *12*, 728783. https://doi.org/10.3389/FIMMU.2021.728783.

65. Rodgers, J.T., Lerin, C., Haas, W., Gygi, S.P., Spiegelman, B.M., and Puigserver, P. (2005). Nutrient control of glucose homeostasis through a complex of PGC-1α and SIRT1. Nature 2005 434:7029 *434*, 113–118. https://doi.org/10.1038/nature03354.

66. Lim, J.H., Lee, Y.M., Chun, Y.S., Chen, J., Kim, J.E., and Park, J.W. (2010). Sirtuin 1 Modulates Cellular Responses to Hypoxia by Deacetylating Hypoxia-Inducible Factor 1α. Mol Cell *38*, 864–878. https://doi.org/10.1016/J.MOLCEL.2010.05.023.

67. Hallows, W.C., Yu, W., and Denu, J.M. (2012). Regulation of Glycolytic Enzyme Phosphoglycerate Mutase-1 by Sirt1 Protein-mediated Deacetylation. Journal of Biological Chemistry *287*, 3850–3858. https://doi.org/10.1074/JBC.M111.317404.

68. Bertschi, N.L., Steck, O., Luther, F., Bazzini, C., von Meyenn, L., Schärli, S., Vallone, A., Felser, A., Keller, I., Friedli, O., et al. (2023). PPAR-γ regulates the effector function of human T helper 9 cells by promoting glycolysis. Nature Communications 2023 14:1 *14*, 1–13. https://doi.org/10.1038/s41467-023-38233-x.

69. Parkhomchuk, D., Borodina, T., Amstislavskiy, V., Banaru, M., Hallen, L., Krobitsch, S., Lehrach, H., and Soldatov, A. (2009). Transcriptome analysis by strand-specific sequencing of complementary DNA. Nucleic Acids Res *37*, e123. https://doi.org/10.1093/NAR/GKP596.

70. Martin, F.J., Amode, M.R., Aneja, A., Austine-Orimoloye, O., Azov, A.G., Barnes, I., Becker, A., Bennett, R., Berry, A., Bhai, J., et al. (2023). Ensembl 2023. Nucleic Acids Res *51*, D933–D941. https://doi.org/10.1093/NAR/GKAC958.

71. Bray, N.L., Pimentel, H., Melsted, P., and Pachter, L. (2016). Near-optimal probabilistic RNA-seq quantification. Nature Biotechnology 2016 34:5 *34*, 525–527. https://doi.org/10.1038/nbt.3519.

72. R Core Team (2024) (2024). R: A Language and Environment for Statistical Computing. Preprint at R Foundation for Statistical Computing.

73. Soneson, C., Love, M.I., and Robinson, M.D. (2016). Differential analyses for RNA-seq: transcript-level estimates improve gene-level inferences. F1000Research 2016 4:1521 *4*, 1521. https://doi.org/10.12688/f1000research.7563.2.

74. Huber, W., Carey, V.J., Gentleman, R., Anders, S., Carlson, M., Carvalho, B.S., Bravo, H.C., Davis, S., Gatto, L., Girke, T., et al. (2015). Orchestrating high-throughput genomic analysis with Bioconductor. Nature Methods 2015 12:2 *12*, 115–121. https://doi.org/10.1038/nmeth.3252.

75. Pagès H, C.M.A.P.F.S.M.M. (2024). txdbmaker: Tools for making TxDb objects from genomic annotations. Preprint.

76. Durinck, S., Spellman, P.T., Birney, E., and Huber, W. (2009). Mapping identifiers for the integration of genomic datasets with the R/Bioconductor package biomaRt. Nat Protoc *4*, 1184–1191. https://doi.org/10.1038/NPROT.2009.97.

77. Chen, Y., Chen, L., Lun, A.T.L., Baldoni, P.L., and Smyth, G.K. (2024). edgeR v4: powerful differential analysis of sequencing data with expanded functionality and improved support for small counts and larger datasets. bioRxiv, 2024.01.21.576131. https://doi.org/10.1101/2024.01.21.576131.

78. Robinson, M.D., and Oshlack, A. (2010). A scaling normalization method for differential expression analysis of RNA-seq data. Genome Biol *11*, 1–9. https://doi.org/10.1186/GB-2010-11-3-R25/FIGURES/3.

79. Ritchie, M.E., Phipson, B., Wu, D., Hu, Y., Law, C.W., Shi, W., and Smyth, G.K. (2015). limma powers differential expression analyses for RNA-sequencing and microarray studies. Nucleic Acids Res *43*, e47–e47. https://doi.org/10.1093/NAR/GKV007.

80. Love, M.I., Huber, W., and Anders, S. (2014). Moderated estimation of fold change and dispersion for RNA-seq data with DESeq2. Genome Biology 2014 15:12 *15*, 1–21. https://doi.org/10.1186/S13059-014-0550-8.

81. Phipson, B., Lee, S., Majewski, I.J., Alexander, W.S., and Smyth, G.K. (2016). Robust hyperparameter estimation protects against hypervariable genes and improves power to detect differential expression. https://doi.org/10.1214/16-AOAS920 *10*, 946–963. https://doi.org/10.1214/16-AOAS920.

82. Liu, R., Holik, A.Z., Su, S., Jansz, N., Chen, K., Leong, H.S., Blewitt, M.E., Asselin-Labat, M.L., Smyth, G.K., and Ritchie, M.E. (2015). Why weight? Modelling sample and observational level variability improves power in RNA-seq analyses. Nucleic Acids Res *43*, e97. https://doi.org/10.1093/NAR/GKV412.

83. Consortium, T.G.O., Aleksander, S.A., Balhoff, J., Carbon, S., Cherry, J.M., Drabkin, H.J., Ebert, D., Feuermann, M., Gaudet, P., Harris, N.L., et al. (2023). The Gene Ontology knowledgebase in 2023. Genetics *224*. https://doi.org/10.1093/GENETICS/IYAD031.

84. Ashburner, M., Ball, C.A., Blake, J.A., Botstein, D., Butler, H., Cherry, J.M., Davis, A.P., Dolinski, K., Dwight, S.S., Eppig, J.T., et al. (2000). Gene Ontology: tool for the unification of biology. Nature Genetics 2000 25:1 *25*, 25–29. https://doi.org/10.1038/75556.

85. Wolf, F.A., Angerer, P., and Theis, F.J. (2018). SCANPY: Large-scale single-cell gene expression data analysis. Genome Biol *19*, 1–5. https://doi.org/10.1186/S13059-017-1382-0/FIGURES/1.

86. Robinson, J.L., Kocabaş, P., Wang, H., Cholley, P.E., Cook, D., Nilsson, A., Anton, M., Ferreira, R., Domenzain, I., Billa, V., et al. (2020). An Atlas of Human Metabolism. Sci Signal *13*, eaaz1482. https://doi.org/10.1126/SCISIGNAL.AAZ1482.

Supplementary Figures

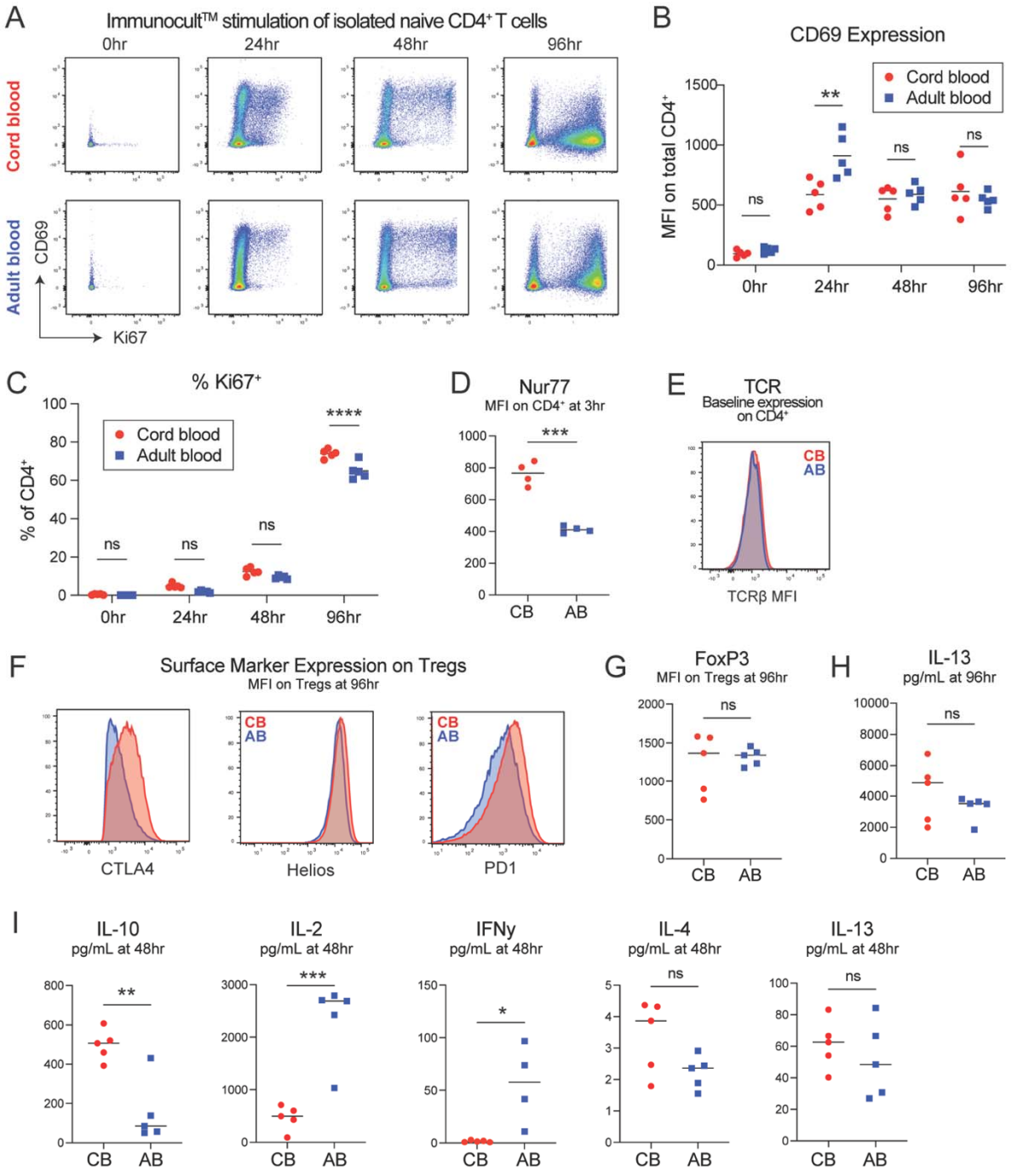

Figure S1: Related to main Figure 1 (A-C) Representative flow plots and quantification of CD69 and Ki67 on total $CD4^+$ population, after naïve $CD4^+$ T cell were isolated from CB and AB and profiled at 0hr (non-stimulated) or 24, 48, and 96hr after TCR stimulation with Immunocult™ anti-CD3/CD28 soluble antibodies. (D) Nur77 mean fluorescence intensity (MFI) in $CD4^+$ T cells from above cultures measured 3hr post stimulation with Immunocult™. (E) TCRβ MFI on naïve $CD4^+$ T cells from CB and AB measured at baseline (0hr). (F) Representative staining pattern of functional Treg markers on $FOXP3^+CD25^+$ (Tregs) emerging from CB and AB naïve $CD4^+$ T cells cultures at 96hr post-stimulation. (G) FOXP3 MFI on these same Tregs at 96hr. (H) ELISA-based measurement of IL-13 in cell culture supernatant of stimulated CB and AB naïve $CD4^+$ T cells at 96hr. (I) ELISA of cytokines in culture supernatant of 48hr post-stimulation.

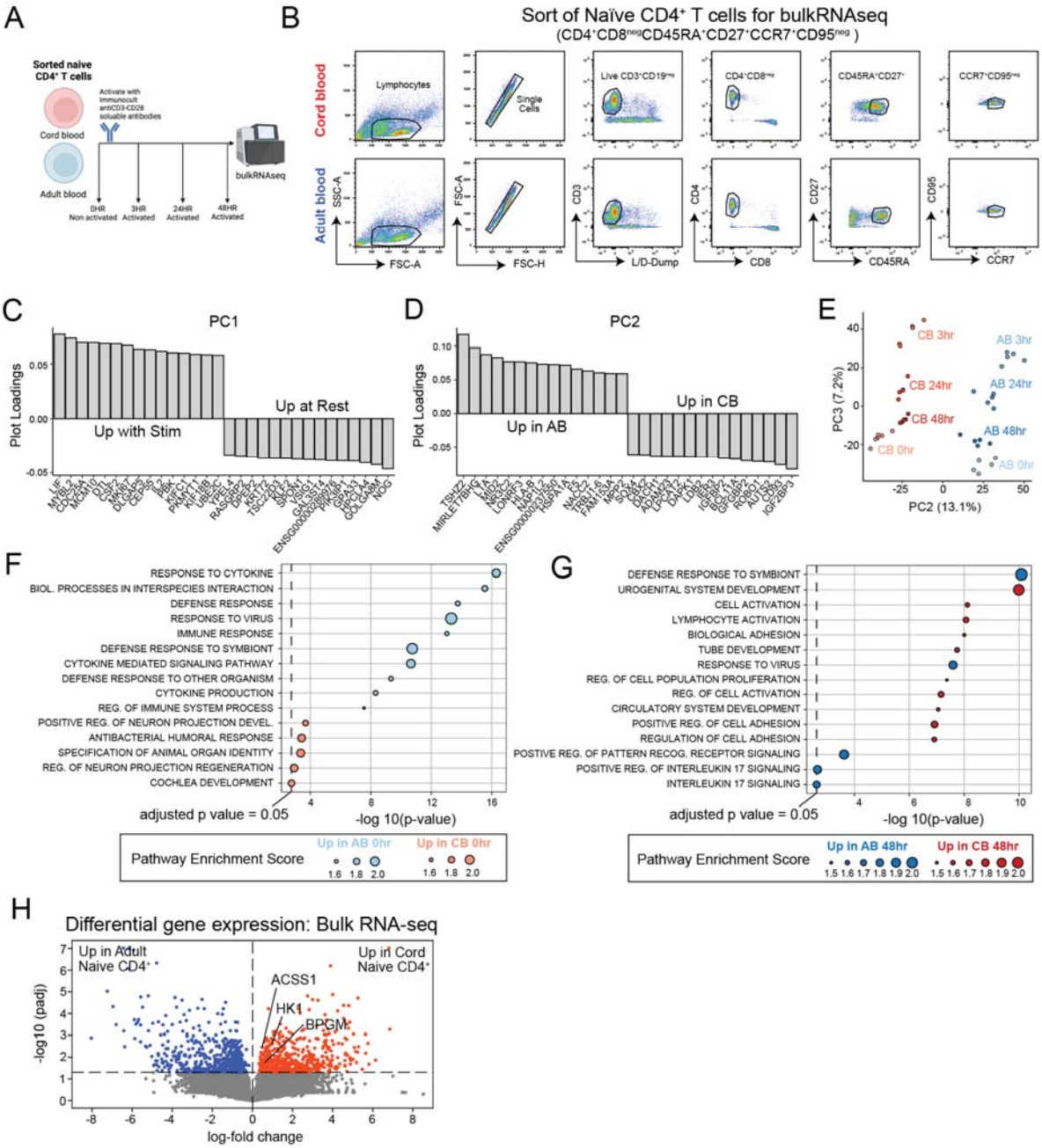

Figure S2: Related to main Figure 2 (A) Schematic of bulk RNA-seq data acquisition. CB and AB naïve $CD4^+$ T cells were isolated via FACS and sequenced at 0hr (baseline, non-activated) or following 3hr, 24hr or 48hr of activation with ImmunoCult^{TM} anti-CD3/CD28 soluble antibodies. (B) Sort strategy for naïve $CD4^+$ T cells from CB and AB for bulk RNA-seq (Live $CD4^+CD8^{neg}CD45RA^+CD27^+CCR7^+CD95^{neg}$). (C) Gene loadings with the greatest contributions to PC1 are associated with activation. (D) Gene loadings with the greatest contributions to PC2 are associated with age. (E) PC2 vs. PC3 from bulk RNA-seq dataset. (F-G) Geneset enrichment analysis on ranked genes in CB vs. AB at 0hr and 48hr. (H) Differential expression analysis on bulk RNA-seq data shows upregulation of certain glycolysis-related genes. Genes with statistically significant differential expression are colored by age.

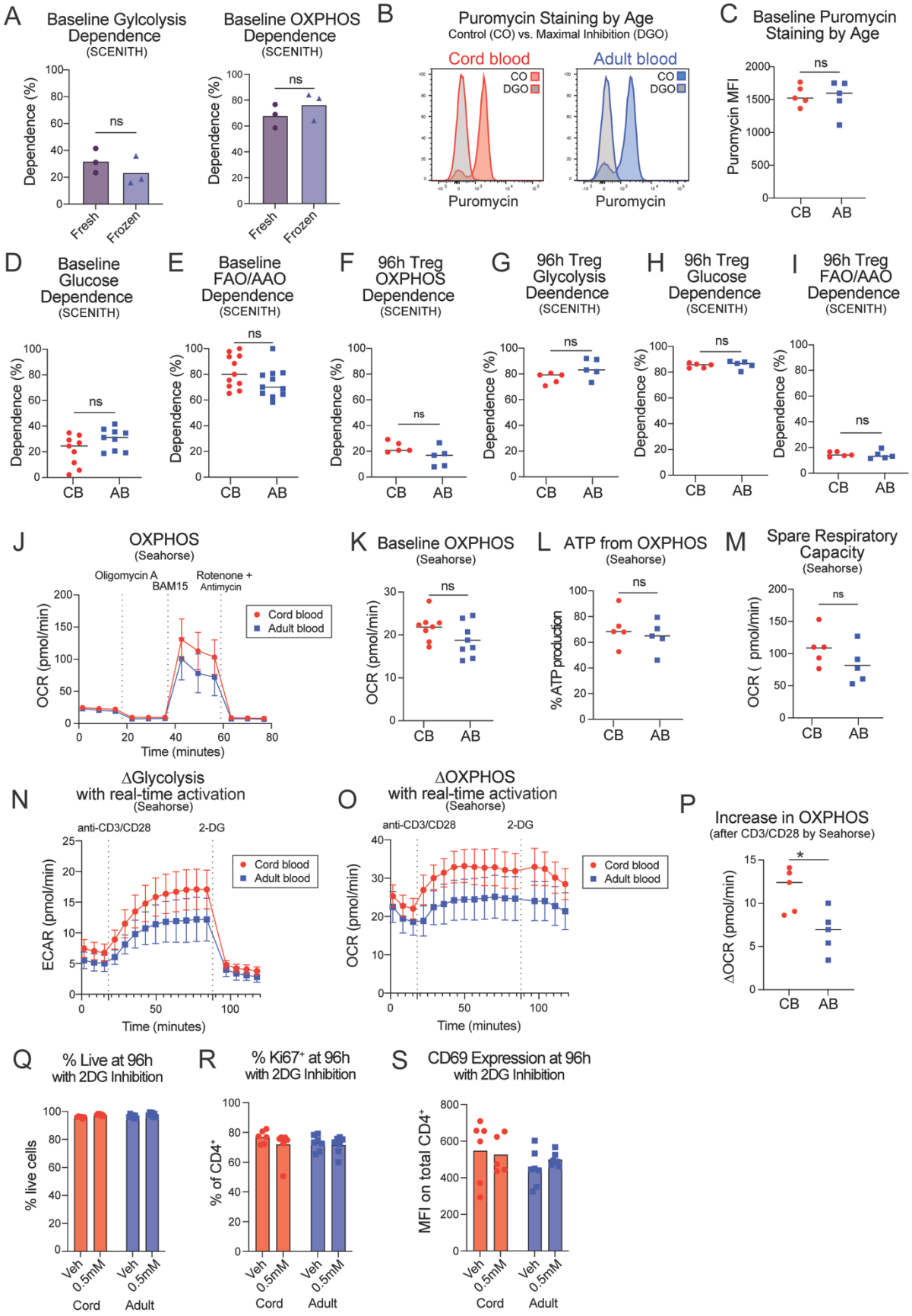
A
Baseline Gylcolysis Dependence (SCENITH)
Baseline OXPHOS Dependence (SCENITH)
Dependence (%)
ns
Fresh
Frozen
B
Puromycin Staining by Age
Control (CO) vs. Maximal Inhibition (DGO)
Cord blood
Adult blood
CO
DGO
Puromycin
C
Baseline Puromycin Staining by Age
Puromycin MFI
CB
AB
D
Baseline Glucose Dependence (SCENITH)
E
Baseline FAO/AAO Dependence (SCENITH)
F
96h Treg OXPHOS Dependence (SCENITH)
G
96h Treg Glycolysis Deendence (SCENITH)
H
96h Treg Glucose Dependence (SCENITH)
I
96h Treg FAO/AAO Dependence (SCENITH)
J
OXPHOS (Seahorse)
Oligomycin A
BAM15
Rotenone + Antimycin
Cord blood
Adult blood
OCR (pmol/min)
Time (minutes)
K
Baseline OXPHOS (Seahorse)
L
ATP from OXPHOS (Seahorse)
% ATP production
M
Spare Respiratory Capacity (Seahorse)
N
ΔGlycolysis with real-time activation (Seahorse)
anti-CD3/CD28
2-DG
ECAR (pmol/min)
O
ΔOXPHOS with real-time activation (Seahorse)
P
Increase in OXPHOS (after CD3/CD28 by Seahorse)
ΔOCR (pmol/min)
Q
% Live at 96h with 2DG Inhibition
% live cells
Veh
0.5mM
Cord
Adult
R
% Ki67+ at 96h with 2DG Inhibition
% of CD4+
S
CD69 Expression at 96h with 2DG Inhibition
MFI on total CD4+

Figure S3: Related to main Figure 3 (A) Baseline (non-activated) dependence on glycolysis and mitochondrial oxidative phosphorylation in fresh and previously frozen adult $CD4^+$ T cells measured via SCENITH. (B) Example staining for SCENITH of puromycin MFI shift with Control vs DGO conditions for baseline (non-activated) CB and AB naive $CD4^+$ T cells. (C) Quantification of puromycin MFI in Control (no metabolic inhibitor condition) for baseline (non-activated) CB and AB naive $CD4^+$ T cells. (D, E) Baseline (non-activated) dependence on glucose and fatty acid/amino acid oxidation in CB and AB naive $CD4^+$ T cells measured via SCENITH. (F-I) Dependence on glycolysis, mitochondrial oxidative phosphorylation, glucose, and fatty acid/amino acid oxidation in CB and AB $FOXP3^+CD25^+$ (Tregs) measured via SCENITH 96 hours after activation. (J) Seahorse graph of OCR (oxidative phosphorylation (OXPHOS)) of baseline (non-activated) CB and AB naive $CD4^+$ T cells. (K) Quantification of baseline OXPHOS between CB and AB naive $CD4^+$ T cells via Seahorse. (L) The percent of ATP made from OXPHOS between CB and AB naive $CD4^+$ T cells via Seahorse. (M) Spare respirator capacity between CB and AB naive $CD4^+$ T cells via Seahorse. (N, O) Seahorse graph of ECAR after acute injection with anti-CD3/CD28 soluble antibodies between CB and AB naive $CD4^+$ T cells via Seahorse. (P) The change in OCR after acute injection with anti-CD3/CD28 soluble antibodies between CB and AB naive $CD4^+$ T cells via Seahorse. (Q) Dose titration of 2DG with quantification of $FOXP3^+CD25^+$ (Tregs) from CB and AB 96 after 24 hours of treatment with 2DG followed by activation with anti-CD3/CD28 soluble antibodies, measured 96 hours after activation. (R, S) Quantification of Ki67+ and CD69 MFI on CD4+ T cells as well as total live cells after 24 hours of treatment with 0.5mM 2DG followed by activation with anti-CD3/CD28 soluble antibodies, measured 96 hours after activation.

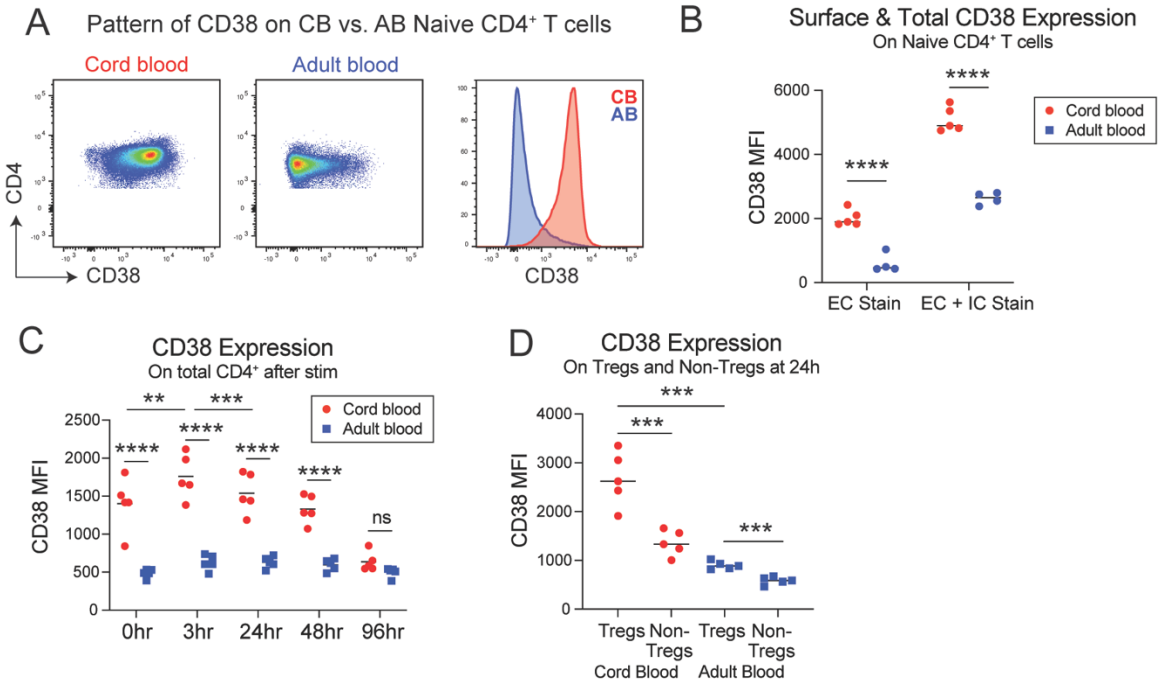

Figure S4: Related to main Figure 4 (A) Staining and MFI difference of CD38 between CB and AB naïve $CD4^+$ T cells at baseline. (B) CD38 MFI on CB and AB naïve $CD4^+$ T cells when stained extracellularly vs extra- and intracellularly. (C) CD38 MFI on $CD4^+$ T cells at 0, 3, 24, 48, and 96hr after activation with anti-CD3/CD28 soluble antibodies. (D) CD38 MFI measured on $FOXP3^+CD25^+$ (Tregs) and $FOXP3^-CD25^-$ (non-Tregs) from CB and AB samples 24 hours after activation.

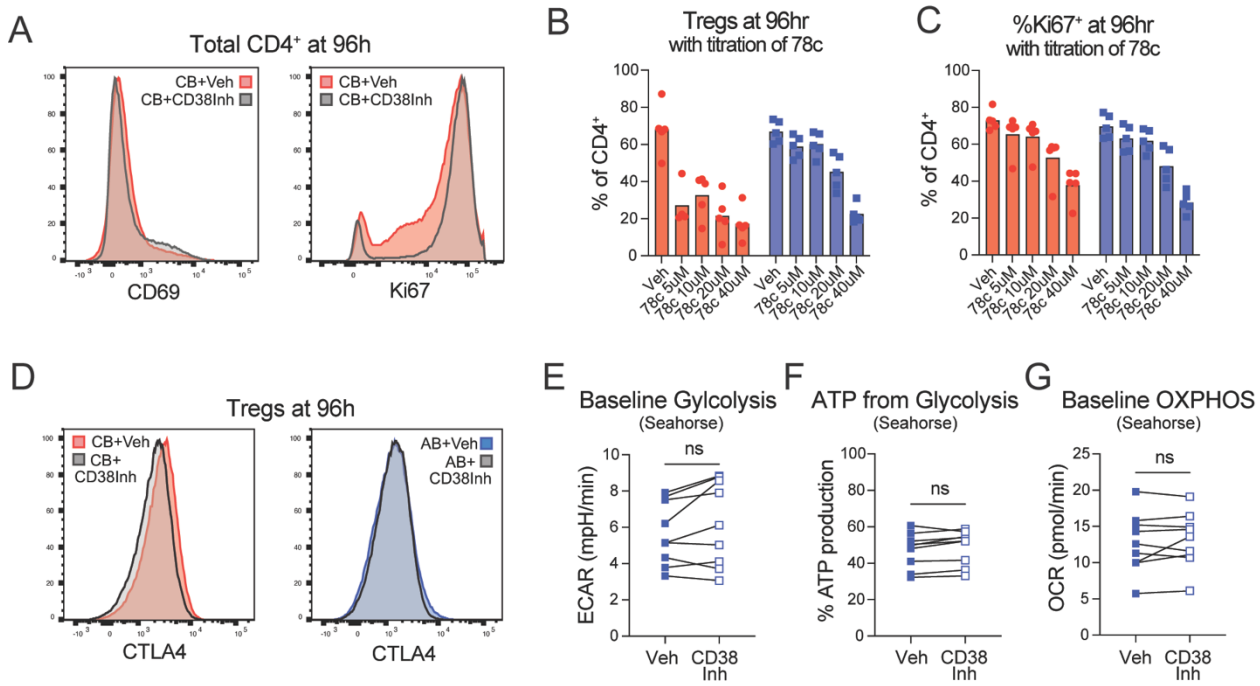

Figure S5: Related to main Figure 5 (A) Representative CD69 and Ki67 MFI plots of $CD4^+$ T cells from cord blood (CB) and adult blood (AB) 96hr stimulated cells with vehicle (DMSO) or CD38 inhibitor (5uM 78c). Cells were treated with DMSO or 78c for 24hr prior to activation and Treg measurement 96hr after stimulation. (B) Quantification of Tregs from titration of CD38 inhibitor 78c. (C) Quantification of $Ki67^+$ $CD4^+$ T cells from titration of CD38 inhibitor 78c. (D) Representative CTLA4 MFI plots of $CD4^+$ T cells from CB and AB 96hr stimulated cells with vehicle (DMSO) or CD38 inhibitor (5uM 78c). (E) Quantification of baseline glycolysis between DMSO and 78c treated AB naive CD4+ T cells via Seahorse. (F) Percent of ATP made from glycolysis for DMSO versus 78c treated AB naive CD4+ T cells via Seahorse. (G) Baseline oxidative phosphorylation of DMSO and 78c treated AB naive CD4+ T cells via Seahorse.